

Tunneling in a Quantum Analog:  
An Experimental Investigation of a Bouncing Oil Drop System

---

A Thesis  
Presented to  
The Division of Mathematics and Natural Sciences  
Reed College

---

In Partial Fulfillment  
of the Requirements for the Degree  
Bachelor of Arts

---

Miguel B. Conner

May 2015



Approved for the Division  
(Physics)

A handwritten signature in black ink, appearing to read "Daniel Borrero", written over a horizontal line.

Daniel Borrero



# Acknowledgements

There are a variety of people who have made this thesis possible. I'd like to start by thanking Daniel Borrero, who advised me this year. Along the way he also showed me the bouncing droplet system, helped me troubleshoot experimental issues, showed me reason, logic, corrected endless drafts, introduced me to John Bush (that's right; John Bush [1]), and a bunch of other things. Thanks Daniel, for being so generous with your time and energy. I'm also greatly indebted to Jay for help with the design and construction of various components of the thesis, and for always having a great attitude. Noah and Bob were also gracious enough to lend me equipment and help overcome a few technical obstacles. Finally, thanks to Lily, Kai, and Jack for reading over my drafts.

More broadly, I owe a lot of my growth, both personal and academic, to a couple of excellent professors at Reed. Most of my physics education can be traced to Daniel, Darrell, Nelia, Johnny, Lucas, Joel, and everyone else in the department. I learned a lot about hard work, lab skills, and physics. In other disciplines, I've had the pleasure of learning from Libby, Albert, Alan, and others who introduced me their subjects and helped me as I stumbled along.

Finally, I'd like to thank all of the people who supported me during my time at Reed. Thanks to Mom and Dad for basically everything. Kai, thanks for being my friend for 4 years, I couldn't have done it without you. You are the best  $\beta$  a guy could wish for. In all seriousness though, I love you. Finally, I have to thank Lily and Clops. They, notably Clops, have been incredibly supportive of everything I have done for the last two and half years.



# Table of Contents

<b>Introduction</b> . . . . .	<b>1</b>
<b>Chapter 1: Pilot-Wave Hydrodynamics</b> . . . . .	<b>7</b>
1.1 Oil Droplet System . . . . .	7
1.1.1 Faraday Waves . . . . .	8
1.1.2 Vibration Number . . . . .	8
1.1.3 Walking . . . . .	9
1.1.4 Path Memory . . . . .	13
1.2 Bouncing Droplets as a Pilot-Wave Analog . . . . .	14
1.2.1 Long Term Droplet Behavior . . . . .	15
1.2.2 Tunneling . . . . .	15
<b>Chapter 2: Experimental Design</b> . . . . .	<b>19</b>
2.1 Setup . . . . .	19
2.2 Materials . . . . .	20
2.2.1 Tray . . . . .	20
2.2.2 Silicone Oil . . . . .	21
2.2.3 Shaker . . . . .	23
2.2.4 Waveform Generator and Amplifier . . . . .	23
2.2.5 Accelerometer . . . . .	23
2.2.6 Shield . . . . .	24
2.2.7 Leveling Platform . . . . .	24
2.2.8 Camera . . . . .	24
2.3 Procedure . . . . .	24
2.3.1 Finding the Walking Regime . . . . .	24
2.3.2 The Experiment . . . . .	25
<b>Chapter 3: Data Analysis and Results</b> . . . . .	<b>27</b>
3.1 Raw Data . . . . .	27
3.2 Analysis . . . . .	28
3.2.1 Tunneling vs. Oil Depth . . . . .	28
3.2.2 Tunneling by Droplet Velocity . . . . .	29
3.3 Sources of Error . . . . .	31
3.3.1 Droplet Diameter . . . . .	32
3.3.2 Droplet Velocity . . . . .	34

3.3.3	Height of Oil . . . . .	35
3.3.4	Consistency of Memory . . . . .	35
3.3.5	Imperfect Droplet Motion . . . . .	35
	<b>Conclusion . . . . .</b>	<b>37</b>
	<b>Appendix . . . . .</b>	<b>39</b>
	<b>References . . . . .</b>	<b>41</b>

# Abstract

In 2005 it was discovered that an oil droplet placed on a vibrating bath of the same oil would bounce along the surface of the oil indefinitely, propelled by the waves it created [2]. This “walker” exhibits many behaviors analogous to those observed in quantum systems, such as single particle double slit diffraction [3], quantized orbits [4], and among others [1], tunneling [5]. Tunneling occurs when a droplet interacts with a submerged barrier; the droplet either passes over or reflects off of the barrier. In experiments described here, we study the dependence of the tunneling probability on the height of a barrier of width  $e = 3.0$  mm. It was determined that tunneling occurred for barriers where the depth of the oil on top of the barrier  $h$  was greater than 1 mm, and showed “quantum-like” probabilistic behavior at an oil depth of  $h = 1.25$  mm. It was also observed that droplets with higher momentum are more likely to tunnel.



# Introduction

“While the founding fathers agonized over the question ‘particle’ or ‘wave’, de Broglie in 1925 proposed the obvious answer ‘particle’ and ‘wave’... [t]his idea seems to me so natural and simple, to resolve the wave-particle dilemma in such a clear and ordinary way, that it is a great mystery to me that it was so generally ignored.” -J. S. Bell

Quantum mechanics is perhaps one of the most counter-intuitive scientific theories in the history of the scientific method. At the atomic level, where quantum effects dominate, the laws that seem to govern our everyday world are no longer relevant. Determinism, the idea that every effect has a cause, is replaced with the idea that every action is probabilistic. A particle cannot be described by precise coordinates; instead, it is described using a wavefunction which provides a range of possible locations with associated probabilities. This probabilistic interpretation of quantum mechanics is known as the Copenhagen interpretation, and represents the most common form of rationalizing the radical, experimental observations of quantum mechanics.

In 2005, Couder et al. showed that oil drops bouncing on a vertically vibrated fluid bath exhibit properties analogous to the paradoxical properties previously seen only at the quantum scale [6]. The system operates at the macroscale, meaning that it is governed by the more “intuitive” classical laws, but still behaves *like* a quantum system. The accessibility of this experiment allows us to observe fundamental, “quantum”-like phenomena in a way that is impossible at the nanoscale. For example, in quantum mechanics, one can never know the position *and* the velocity of a particle, simply because it can never *have* a perfectly defined position and velocity. In this experiment, however, the “particle” can be easily seen at all times, so both its position and velocity can be easily tracked.

The behavior of the droplet system seems to agree with a theory of quantum mechanics proposed by Louis de Broglie in 1923 known as pilot-wave theory [7, 8]. Unlike the probabilistic viewpoint subscribed to by adherents of the Copenhagen interpretation, de Broglie’s model asserts that the particle *has* a precise location, and that the particle is pushed by a guiding or “pilot” wave. The theory was extended by David Bohm in 1952 [9, 10], but never caught on because it gained “realism” (the idea that a particle is well defined at all times) at the expense of “locality” (the idea of a universal speed limit where nothing, including information, can travel faster than the speed of light required by special relativity); a trade that is generally considered

unfavorable by physicists.<sup>1</sup>

De Broglie's original theory is underdeveloped, having remained relatively obscure for the better part of the last century. Since the predictions of the Copenhagen interpretation and de Broglie's theory are similar, experiments have done little to clarify the debate. As a result, the more developed Copenhagen school of thought holds its place as *the* interpretation of quantum phenomena.

After taking a course in quantum mechanics, I found it difficult to truly believe some of the associated implications of the Copenhagen interpretation. I was seduced by some of the more obscure quantum methodologies that promised salvation from indeterminism and non-realism (such as Bohm or de Broglie's theories), and it was difficult from me to resist the opportunity to investigate analogs of these methodologies in an experimental setting. The bouncing droplet system, which serves as a hydrodynamic quantum analog and forms the backbone of this thesis, is introduced below.

## Bouncing Droplets

Though it had been observed for at least a century, the phenomena of droplets bouncing on a fluid bath was first explained by Jearl Walker in 1978 [11]. The investigations began with a simple droplet of water falling onto a bath of water and remaining just a second too long before coalescence.<sup>2</sup> Walker discovered that by adding detergent to the water and vibrating the bath, he could extend the lifetime of the droplets from fractions of a second to several minutes. These droplets bounce at frequencies of around 50 Hz (50 bounces per second) and are very small, with a diameters of a millimeter or less. These two factors make it difficult to observe even the main mechanisms that drive the behavior. A key insight by Walker was that by flashing a strobe light at a frequency slightly slower than the rate of vibration of the bath, he could observe the droplet bouncing as if in slow motion.

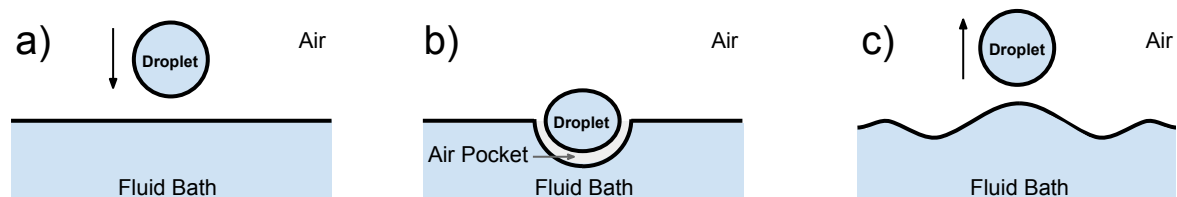


Figure 1: A depiction of a droplet bouncing on a bath of the same fluid. (a) A droplet falls onto a fluid bath. (b) A film of air gets trapped underneath the droplet. (c) The droplet bounces back up off of the cushion of air leaving behind waves that propagate radially.

Walker found that a trapped film of air kept the droplet and the bath from touching, as shown in Fig. 3. That is, the droplet is bouncing on a layer of air that is being pushed out from under the droplet, but because the bounce happens so quickly, the

<sup>1</sup>The Copenhagen interpretation of quantum mechanics, by the way, is non-realist and non-local.

<sup>2</sup>It is often reported that this occurs in coffeemakers, as the coffee drips into the pot.

fluid droplet and the fluid bath never touch. Walker concluded that the leakage rate of this trapped pocket of air depends on three factors: the surface tension of the fluid in the bath, the viscosity of the droplet and the fluid bath, and the viscosity of air. He found that the bath must be of uniform surface tension and free from floating particulate matter, since both could lead to coalescence. Higher viscosity fluids led to longer droplet lifetimes, since more viscous fluids make it more difficult for air to escape the gap between the drop and the bath. Finally, adjusting the frequency and the amplitudes of the vibrations also affected droplet lifetime.<sup>3</sup>

More recent research showed that droplets of fluids like silicone oil can bounce indefinitely on a vibrating bath [2]. The long lifetime occurs not only because silicone oil has a high viscosity, but also because it has a *low* surface tension. A low surface tension is beneficial because it makes the oil bath relatively immune to surfactants (e.g. detergent) or contamination that would otherwise make the surface tension nonuniform and lead the drop to coalescence.

## Faraday Waves

The behavior of a fluid in a vertically vibrated bath can be controlled by adjusting the amplitude or the frequency of the vibration. Depending on a variety of factors (size of bath, fluid in bath, etc.) each system has a specific amplitude (given a specific frequency), which if surpassed, will produce standing surface waves called Faraday waves [12].<sup>4 5</sup> A vibrating bath below this critical amplitude, also known as the Faraday threshold, will have a quiescent surface. A bath driven at an amplitude greater than the Faraday threshold will have a turbulent surface with ripples and waves. An example of Faraday waves is shown in Fig. 2. Adjusting the frequency above the Faraday threshold will change the size and shape of the Faraday waves. Note that Faraday waves can be created either by increasing the driving amplitude above a critical level, or adjusting frequency.

## Walking Droplets

A bouncing droplet will bounce differently depending on the frequency and amplitude of the vertical vibrations. If the parameters are set just below the Faraday instability, a curious motion arises: the droplet seems to “walk” across the surface of the oil. The droplet is being pushed by its own ripples, a dual effort in which neither can exist without the other. In essence, the walker is both a particle and a wave; a conjunction reminiscent of the quantum scale.

---

<sup>3</sup>Reedie Andrew Case ('92) wrote his thesis “Oil on Troubled Water: The Extension of Floating Drop Lifetimes Due to Interface Vibration” where he looked at droplet lifetime as a function of vibrational frequency.

<sup>4</sup>Faraday waves were not actually discovered by Michael Faraday; in the footnotes of his paper he cites that they were first observed by Oersted, Wheatstone, Weber, and others. Faraday was just the first to study their behavior in detail.

<sup>5</sup>Another Reed thesis, this one titled “Good Vibrations: A Visual Exploration of Faraday Waves” by Alison Saunders empirically tested the mathematical Faraday wave model.



Figure 2: A picture of Faraday waves in a dish of water at 80 Hz.

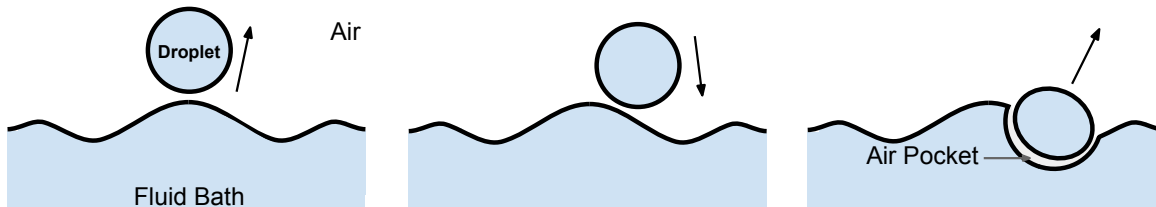


Figure 3: A depiction of a droplet walking across a bath of the same fluid.

## Overview

Recently, two main groups have been investigating the properties of this unique system. A group at Laboratoire Matière et Systèmes Complexes (MSC) in Paris, France, headed by Yves Couder was the first to uncover some of the inherently “quantum”-like behavior of bouncing droplets, in 2005 [6]. Since 2010, John Bush’s group at MIT have created a mathematical model and performed their own investigations of the walker system. Couder, Bush, and others have shown that this system can reproduce double-slit single-particle interference [3], tunneling [5], quantized orbits [4], and many other “quantum”-like effects [1].

This thesis documents an experimental investigation into the “tunneling” behavior of this bouncing droplet system. In this setting, tunneling occurs when the droplet interacts with a submerged barrier. Only one other study looks at this aspect [5], but falls short of completely examining the tunneling behavior, focusing on the effect of barrier width and not examining barrier height. I hope to add to the body of work in this subfield by studying how barrier height affects probability of tunneling.

This thesis is divided into three main chapters. **Chapter 1** describes the hydrodynamic quantum analog along with a brief survey of the relevant literature. **Chapter 2**

---

describes the experimental design and explains the setup and the data acquisition procedures. **Chapter 3** presents the data from my experiments. Finally, the **Conclusion** highlights the results, summarizes the limitations, and suggests avenues for future study.



# Chapter 1

## Pilot-Wave Hydrodynamics

In this chapter I will present a brief survey of the literature describing hydrodynamic quantum analogs, and discuss in more detail the tunneling experiments relevant to my investigation. Because the system was discovered in 2005, most of the literature examining this topic was written within the last decade.

### 1.1 Oil Droplet System

Consider a fluid of density  $\rho$ , viscosity  $\nu$ , and surface tension  $\sigma$  in a bath of depth  $H$ . The bath is sinusoidally driven vertically with an amplitude  $A_0$  at a frequency  $f = \omega/2\pi$ . By defining  $\gamma = A_0\omega^2$ , the effective gravity in the frame of reference of the bath is  $g + \gamma \sin(\omega t)$ . The surface of fluid in the shaking tray remains quiescent for lower values of  $\gamma$ . However, if  $\gamma$  is increased above a certain threshold (by increasing  $A_0$  or  $f$ ), the surface becomes unstable leading to the appearance of standing surface waves called Faraday waves. We define this threshold as the **Faraday threshold**,  $\gamma_F$ . The value of  $\gamma_F$  changes depending on the size and shape of the tray, the amount of fluid in the tray, as well as the properties of the fluid.

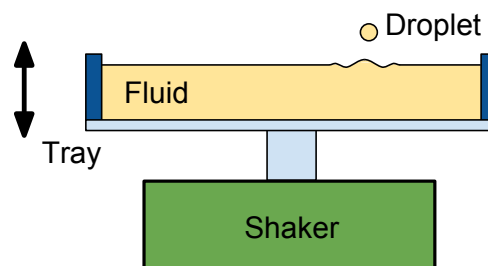


Figure 1.1: A droplet bounces on a vertically vibrating fluid bath. The tray vibrates with an amplitude  $A_0$  at frequency  $f$ .

If we take a toothpick and break the surface of the vibrating oil bath, we form a droplet of oil of diameter  $D$  as shown in Fig. 1.1 that bounces on the surface for hours. The droplet bounces on a pocket of air, which is trapped beneath the droplet and the bath [11]. As the oil droplet bounces, it creates radially traveling waves that

propagate outwards on an otherwise flat surface. The droplet will continue bouncing for a specific range of values of  $\gamma$ . For small  $\gamma$ , the forcing is not enough to sustain the droplet, and it quickly coalesces. Increasing  $\gamma$  above the threshold for coalescence leads to a variety of different bouncing regimes until at  $\gamma = \gamma_F$  where Faraday waves emerge. Below  $\gamma_F$ , the value of  $\gamma$  also affects the range of the radial waves; for low  $\gamma$ , these waves quickly dissipate, but as  $\gamma$  approaches  $\gamma_F$ , they are sustained longer. We are interested in studying the region below the appearance of Faraday waves but above the region of coalescence. The range of the various parameters which allow for the existence of bouncing droplets are outlined in Table 1.1.

Table 1.1: Approximate limits for bouncing drop behavior. The value  $g = 9.81 \text{ m/s}^2$  is the standard acceleration due to gravity. Adapted from [1].

Parameter	Lower Limit	Upper Limit
Viscosity $\nu$ (cSt)	10	100
Bath Depth $H$ (mm)	4	10
Frequency $f$ (Hz)	20	150
Amplitude $A_0$ (mm)	0.1	1
Drop Diameter $D$ (mm)	0.6	1.0
Forcing Acceleration $\gamma$ ( $\text{ms}^{-2}$ )	$0.5g$	$\gamma_F \approx 4.2g$

### 1.1.1 Faraday Waves

Driving a fluid-filled tray with forcing acceleration  $\gamma = \gamma_F$  we see the appearance of standing surface waves known as Faraday waves. These waves oscillate with a frequency  $f_F = f/2$  and an angular frequency  $\omega_F = 2\pi f_F = \pi f$ . For a fluid bath of density  $\rho$ , surface tension  $\sigma$ , and depth  $H$ , the standing wave and water dispersion relation:

$$\omega_F^2 = \left( gk_F + \frac{\sigma k_F^3}{\rho} \right) \tanh(k_F H), \quad (1.1)$$

can be used to find the wavelengths of standing waves at the Faraday threshold. This relates the angular Faraday frequency  $\omega_F$  to the Faraday wavenumber  $k_F$ , where  $g$  is the gravitational constant [13]. From the wavenumber, we can calculate the wavelength  $\lambda_F$  of the Faraday waves by the relation  $\lambda_F = 2\pi/k_F$ . Though we are interested in investigating the region  $\gamma < \gamma_F$  for which there are no standing surface waves, Eq. (1.1) provides an estimate of the wavelength and frequency of the localized waves surrounding the droplet for the bouncing behavior.

### 1.1.2 Vibration Number

In an experiment of this nature, one usually pours a specific volume of oil in the tray, fixing the values of  $\nu$ ,  $\sigma$ , and  $H$ . One is then left with the option to adjust  $\gamma$

which produces a range of droplet motions, including a slew of different stationary bouncing modes and linear or chaotic “walking” trajectories (which are discussed in Section 1.1.3). To categorize the various bouncing behaviors, we use the vibration number  $V_i$ , which takes into account many of the parameters of the experiment [14]. The vibration number is the ratio of the forcing frequency and the droplet’s natural oscillation frequency  $\omega_D$  and is given by:

$$V_i = \frac{\omega}{\omega_D}, \quad (1.2)$$

where  $\omega_D$  represents the oscillation frequency of a fluid droplet. Rather than remain a perfect sphere, the droplet stretches and contracts vertically as it bounces, and  $\omega_D$  describes the frequency of this motion. The oscillation frequency of a fluid droplet is defined as:

$$\omega_D = 2\sqrt{\frac{2\sigma}{\rho D^3}}, \quad (1.3)$$

where  $\sigma$  is the surface tension,  $\rho$  the density, and  $D$  the diameter of the droplet [15]. Combining Eqs. 1.2 and 1.3 we arrive at:

$$V_i = \frac{\omega}{2} \sqrt{\frac{\rho D^3}{2\sigma}}, \quad (1.4)$$

a dimensionless parameter that captures the effects of the fluid’s material properties, the tray’s vibration, and the droplet’s diameter. Depending on the vibration number  $V_i$  and the driving strength  $\gamma/g$ , the droplets switch between different bouncing states as shown in Fig. 1.2. If we hold the working fluid and the driving frequency constant ( $\sigma$ ,  $\rho$ , and  $\omega$ ), then we can think of increasing  $V_i$  as increasing droplet diameter  $D$ .

The various modes seen in Fig. 1.2 can be described by a pair of numbers  $m$  and  $n$ , where  $n$  is the number of times the droplet contacts the surface over a time span  $m/f$ . For example, in the (1,1) “bounce” mode, the droplet hits the oil bath once per up-and-down motion of the tray. In the (2,2) mode, the drop makes two bounces of differing heights for two driving periods. The “chaos” regimes indicate that the bouncing of the droplet is chaotic and does not exhibit a periodic bouncing motion. The “walk” regime describes a very particular kind of behavior in which the droplet moves forward as it bounces, seemingly walking across the surface. Like bouncing, walking also comes either the (2,1), (4,2), or chaotic modes. Finally, the “coalescence” region demarcates the values for which the droplet coalesces with the bath.

The phase diagram shown in Fig. 1.2 provides a valuable starting place for an experiment since it outlines the many possible states of the system, and where we can expect to find particular behaviors. We will now narrow our focus to only the walking regime, which is the focus of this thesis.

### 1.1.3 Walking

A walking droplet is a very specific type of bouncing droplet that arises between  $\gamma_W < \gamma < \gamma_F$ , where  $\gamma_W$  the the walking threshold. As the droplet bounces vertically

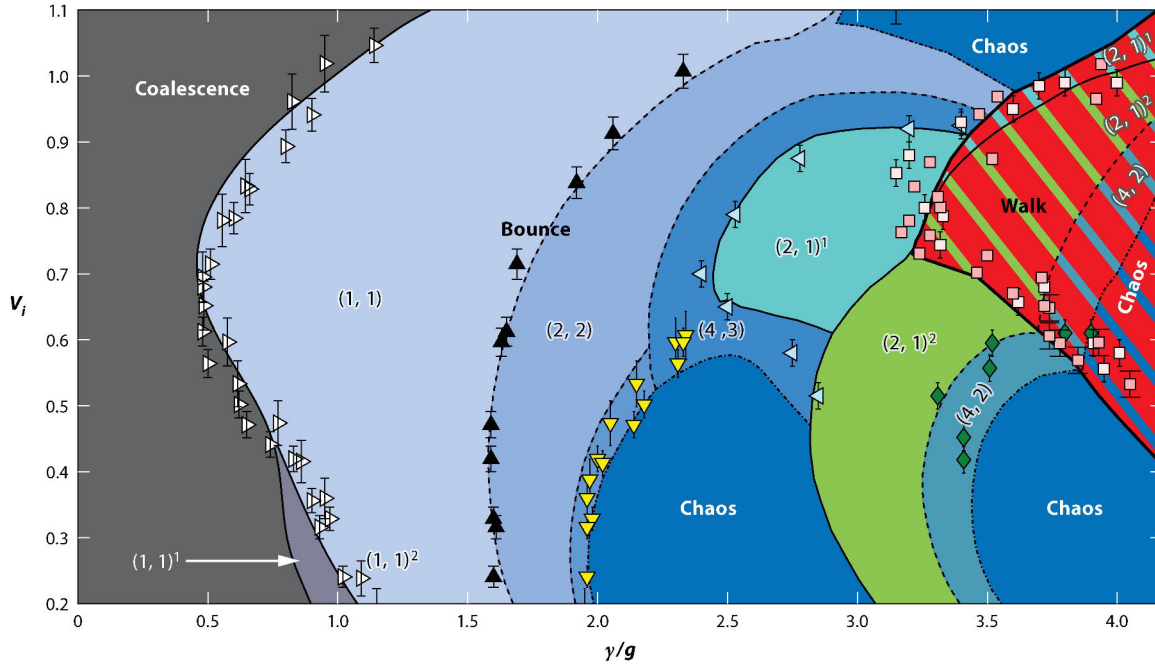


Figure 1.2: The different bouncing regimes for the oil drops of 20 cSt silicone oil at  $f = \omega/2\pi = 80$  Hz, characterized by the non-dimensional forcing amplitude  $\gamma/g$  and the vibration number  $V_i$ . The solid colors represent the modes predicted by a theoretical model [14], and the various points represent experimentally measured limits. The parameters  $(m, n)^i$  describe a droplet that bounces  $n$  times in  $m$  forcing periods, where  $i$  distinguishes modes with different mechanical energy. The Faraday threshold is  $\gamma_F = 4.2$ . Adapted from J. W. M. Bush, *Annu. Rev. Fluid Mech.* **47**, 273 (2015).

on the vibrating fluid bath, the interaction with the wave it generated during its previous bounce gives it a slight horizontal motion. Thus, for every bounce, the droplet follows a parabolic trajectory. But because these droplets are bouncing at 40 times per second (or more) and the parabolic motion is periodic, the vertical oscillations are difficult to see. The apparent behavior that emerges is that of the droplet moving in a straight line along the surface of the fluid bath.

The horizontal component of the walking motion is due to the droplet landing slightly off center from the radial wave it produced in the previous bounce, as shown in Fig. 1.3. At such close proximity to the Faraday threshold, the waves surrounding the droplet are not just regular ripples, but rather are like localized Faraday waves temporarily sustained by the vibrations before decaying away. The kinetic energy from the falling droplet is enough to perturb the unstable surface such that the waves appear, and then the energy introduced by the vertical forcing of the tray keeps these waves from damping out completely, as they would in an un-forced system. The value of  $\gamma$  determines how long these local Faraday waves are sustained. As these waves interfere with one another they create an overall wave field that guides the droplet. This overall wave field is referred to as the **guiding wave** or the **pilot wave**. A

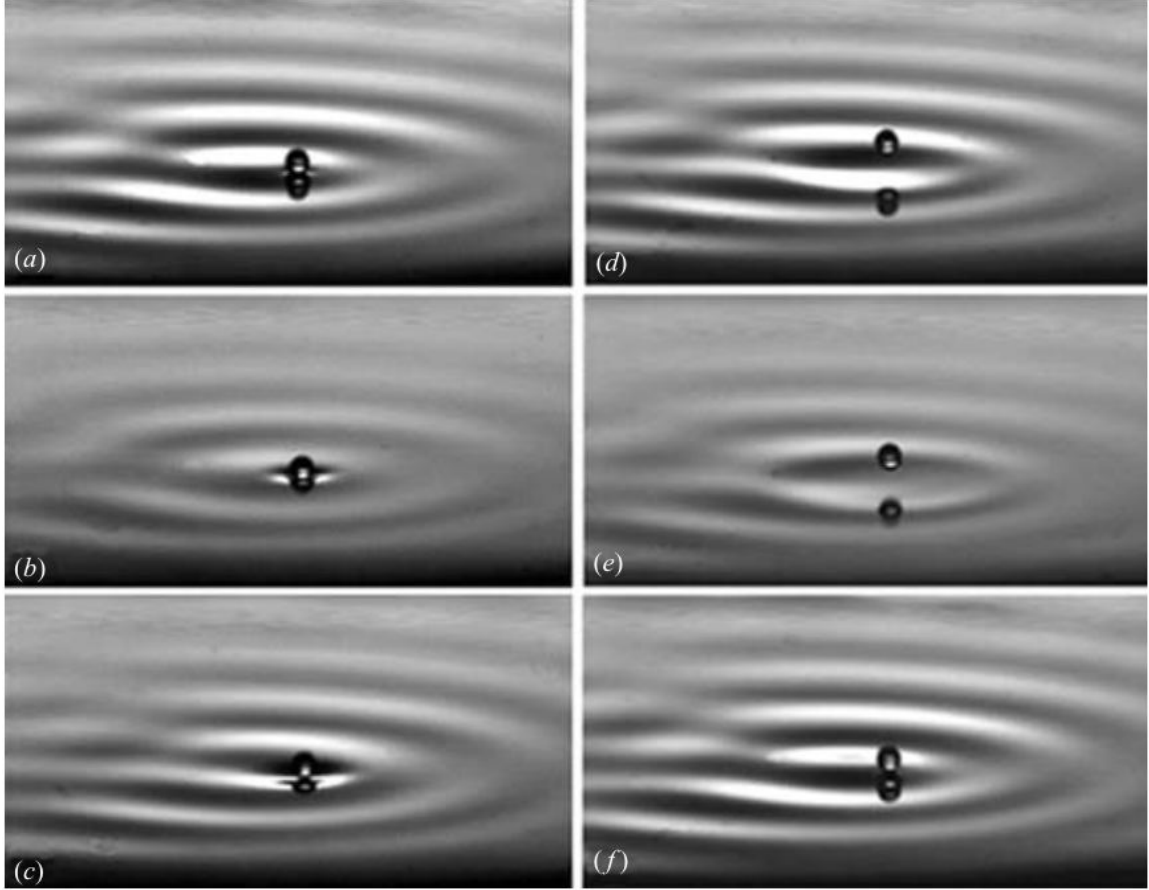


Figure 1.3: The series of pictures (a) - (f) show a walker over two forcing periods. The droplet bounces off of the slope of the localized wave, launching into the air, and then falls again on a new wave slope. This periodic process happens multiple times per second, giving the droplet the appearance of walking across the surface. Figure from S. Protiere et al., *J. Fluid Mech.* **554**, 93 (2006).

**walker** is defined as a self-propelling droplet *and* its guiding wave, since they are mutually interdependent; the droplet creates the guiding wave, and the guiding wave moves the droplet. The unique combination of the two components can result in novel interactions such as bound or scattering states.

### Bound States

A periodic damped wave allows for two bouncers to form a **bound state**: a configuration in which the droplets remain a fixed distance apart [16]. Starting far away from one another, two droplets drift towards one another until a fixed distance  $d_0^{bd}$ . Increasing driving acceleration  $\gamma$  decreases their separation distance  $d_0^{bd}$  (Fig. 1.4). These bound bouncers can form triangular lattices, although their periodicity is highly sensitive to the mass of the droplets. If the masses of the droplets differ, these configurations drift slowly and rotate because the waves produced by the larger droplet create an imbalanced wave field [17]. Finally, the droplets can bounce

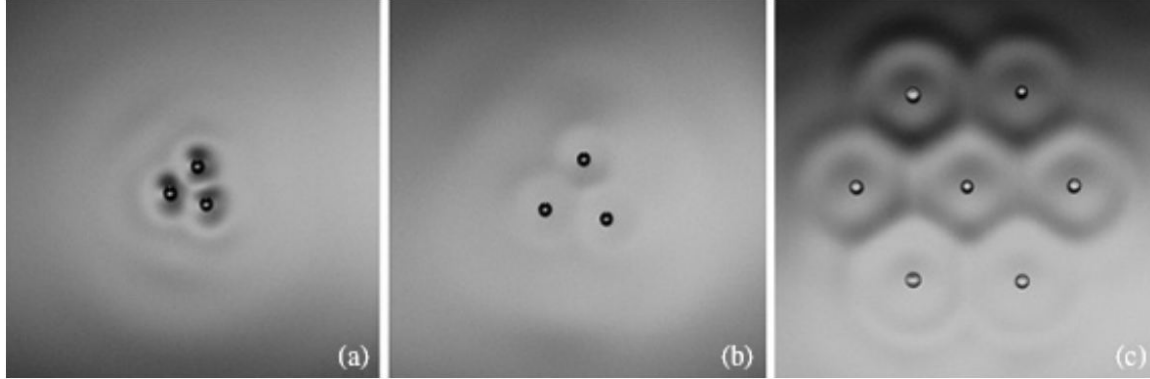


Figure 1.4: In (a), the trio of droplets organize themselves into a triangular lattice separated by distance  $d_0^{bd}$ . The forcing acceleration has been increased in (b), and the droplets are more spread out with a larger  $d_0^{bd}$  value. Bound states can include a large number of bouncing droplets, as demonstrated by the 7 bouncing droplets shown in (c). Figure from S. Protiere et al., *J. Phys.: Condens. Matter* **17**, S3532 (2005).

in phase with one another (they both land at the same time and reach their peaks at the same time) or completely out of phase with one another (as one lands, the other reaches its peak).

Walkers can also form bound states. Two walkers of the same size that are approaching one another can form an orbit around their center of mass as shown in Fig. 1.5. Between the two droplets is the fixed distance  $d_n^{orb}$  given by

$$d_n^{orb} = (n - \epsilon_0)\lambda_F \quad (1.5)$$

where  $\lambda_F$  is the wavelength of the localized Faraday waves estimated by Eq. (1.1),  $\epsilon_0$  is a fixed distance which is the same for all orbitals of these walkers (usually in the range  $0.15 < \epsilon_0 < 0.25$  depending on droplet diameter), and  $n = 1, 2, 3, \dots$  for drops that are in phase or  $n = 1/2, 3/2, 5/2, \dots$  for drops out of phase. Orbiting periods are approximately proportional to  $d_n^{orb}$ , which ends up meaning that the velocity of the orbiting walkers is a little less than the velocity of a free walker [18].

## Scattering States

Two identical walkers headed towards each other can form fixed orbits, or they can scatter. **Scattering** describes an interaction in which droplets are deflected through their wave fields, and never actually make contact with one another. Most of the interactions of a walker are scattering of some form. For example, if a single walker approaches the wall of the tray, it will never actually touch the wall. Instead, the guiding wave reflects off of the wall and modifies the wave field in such a way that the droplet will scatter in the opposite direction.

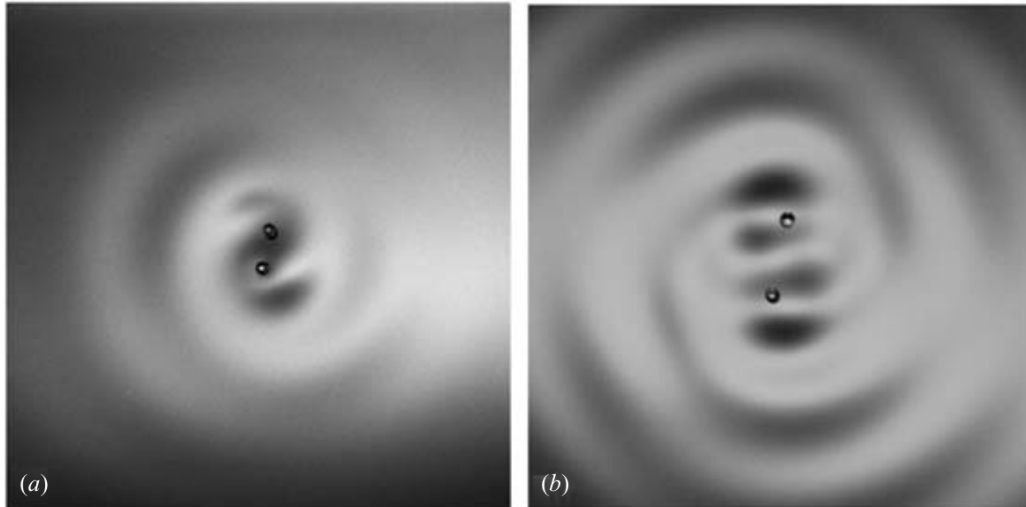


Figure 1.5: The figures show two droplets of equal size orbiting their center of mass. In (a) the droplets bounce out of phase with  $n = 0.5$  and  $d_n^{orb} = 1.65$  mm whereas in (b) the droplets bounce in phase with  $n = 1$  and  $d_n^{orb} = 3.7$  mm. Figure adapted from S. Protiere et al., J. Fluid Mech. **554**, 101 (2006).

#### 1.1.4 Path Memory

The system's proximity to the Faraday threshold is captured by a parameter called path memory. This captures the importance of damping in the system [19]. Every time the droplet impacts the bath, it creates a radial traveling wave. Over the course of many bounces, a guiding wave field composed of a superposition of the many waves arises. In this way the wave field “remembers” previous interactions, but is at the same time being periodically “updated” with every new bounce of the droplet. Because droplet motion is influenced by the wave field, controlling the damping of the wave field influences the path of the walker.

For a bouncing droplet in which the guiding waves decay relatively quickly, the droplet can only be influenced by relatively recent waves. This kind of behavior is characterized as having a low memory. Conversely, a high memory system is one in which waves do not decay quickly; they propagate outwards and reflect off of the surfaces of the tray and interfere with the other waves produced by the droplet. As one gets closer to the Faraday threshold, one achieves higher and higher memory because waves last longer. The quantum-like features described here arise in the high-memory limit.

The non-dimensional memory parameter is formally defined as:

$$M_e = \frac{T_d}{T_F(1 - \gamma/\gamma_F)},$$

where  $T_d$  is the decay time of waves in the absence of vibration and  $T_F$  is the period of the Faraday waves ( $T_F = 1/f_F$ ) [20]. It will suffice to discuss memory as a fraction of the Faraday threshold  $\gamma/\gamma_F$ , since the fraction and  $M_e$  are monotonically related. As the value of  $\gamma/\gamma_F$  increases, we get closer to the Faraday threshold and  $M_e$  increases.

Eventually as  $\gamma/\gamma_F$  approaches 1, the memory parameter approaches  $+\infty$ . Thus, higher forcing  $\gamma$  goes hand in hand with higher memory  $M_e$ .

In practice, walking arises above a value of  $\gamma/\gamma_F = 0.94$ , with more quantum-like phenomena arise at values of  $\gamma/\gamma_F = 0.97$  and above [4]. Deviations in memory  $\gamma/\gamma_F$  as small as  $\pm 0.01$  have been shown to have drastic differences in both long term and short term droplet behaviors [20].

## 1.2 Bouncing Droplets as a Pilot-Wave Analog

The bouncing droplet system discussed above has remarkable similarities to a theoretical model of quantum mechanics. We start by introducing classical mechanics, which seeks to mathematically describe the motion of relatively large scale objects under action of forces. It was, until the late 19th century, physics. Physicists in the early 20th century, after a series of very puzzling experimental results, slowly began to realize that matter at the small scale behaved very differently than what they had been studying in the macroscale world. Quantum mechanics was developed, from the ground up, with the aim of mathematically describing this brave new world. As with any new behavior, a variety of theoretical explanations with mathematically different foundations were tossed around, until, at the 1927 Solvay conference, the Copenhagen interpretation of quantum mechanics emerged. The Copenhagen interpretation was spearheaded by Niels Bohr and Werner Heisenberg, and provides a way of interpreting the mathematics of quantum mechanics. This interpretation is fundamentally probabilistic. In the modern day, most physicists teach and preach the Copenhagen interpretation of quantum mechanics because it is in excellent agreement with experiment and it also is more developed than other interpretations.

The oil droplet system is classical, but it is unique in that it is a classical system that behaves *like* a quantum system. Experimentally, it exhibits a variety of counter-intuitive interactions similar to those seen in quantum mechanical systems [21]. These include single particle double slit diffraction [3], quantized orbits, tunneling (discussed in Section 1.2.2) [5], and others [1]. These unique features stem from the **particle-wave duality**, a central concept in quantum mechanics: the idea that a particle can behave like a particle in some circumstances and like a wave in others. In the hydrodynamic pilot-wave system, this is represented by the walker which is both a droplet and a wave.

The oil droplet system is slightly different than the actual quantum conception since the walker is a droplet *and* a wave, while the Copenhagen interpretation describes an electron (for example) as a particle *or* a wave. In this sense the oil droplet system is not analogous to the Copenhagen interpretation of quantum mechanics. However, it bears remarkable resemblance to a theory proposed by L. de Broglie in 1923, the so-called “double solution” theory [7]. De Broglie proposed that the particle is guided by two waves: a pilot wave created by internal particle oscillations that affects the immediate behavior of the droplet (i.e. the localized Faraday waves) and evolves according to the Klein-Gordon equation, and a wave outlined by the Schrödinger equation that describes the long term statistical behavior of the

droplet's location over time (discussed in Section 1.2.1) [8]. The second statistical wave describing the long term motion of the particle in de Broglie's theory is the very same wave that describes the particle's probable location using the Copenhagen interpretation, but because of de Broglie's extra pilot wave, the same wave is interpreted differently. Unfortunately, because de Broglie could never find the equation of the pilot wave, he could not proceed with his theory and it fell into obscurity. His theory was picked up and modified by David Bohm in 1952 [9, 10], who combined the statistical wave and the guiding wave into a single wave. By combining the two waves, Bohm's formulation loses its relevance to the bouncing droplet system.

It is worth noting that there are a few differences between the hydrodynamic system and an actual quantum system. First of all is the scale; the bouncing droplet system moves under the laws of the macroscopic world. Secondly, the hydrodynamic system is dissipative (waves are damped) and sustained only through continuous energy input (constantly being vibrated), so it is not a conservative system. With that said, it is still worth comparing the two since they appear similar in many other respects.

Despite these differences, it is worth investigating the hydrodynamic pilot-wave analogs in greater detail. We will narrow our focus once again, and investigate the tunneling behavior of this system, which describes the droplet's interaction with sub-surface barriers. The following section explains tunneling in quantum mechanics, and the analogous behavior in the droplet system.

### 1.2.1 Long Term Droplet Behavior

Constraining a walker to a circular region, Harris et al. tracked the motion of the walker over a long period of time [20]. In the high-memory, chaotic motion regime, the droplet was allowed to walk freely while its position was tracked (Fig. 1.6(a)) and translated into the histogram (Fig. 1.6(b)). The histogram provides the probability of finding the walker at a specific location within the corral, and recovers the shape of the Faraday wave that occurs at the Faraday threshold. This histogram serves the same purpose as de Broglie's statistical wave described by the Schrödinger equation. In the Copenhagen interpretation of quantum mechanics, however, this statistical wave (called the wavefunction) fully defines the particle.

### 1.2.2 Tunneling

#### Tunneling in Quantum Mechanics

Among the various phenomena associated with quantum mechanics, tunneling is one of the most surprising. At the classical level, we can take the example of a basketball thrown at a brick wall: the ball will hit the wall and bounce back every time we try it. When we shift to the quantum scale, if we have a particle headed towards a barrier of a given potential energy, it will not necessarily bounce back. Depending on the characteristics of this potential, there will be a few times in which the particle will **tunnel** through the barrier, shooting out on the other side. It is not completely fair

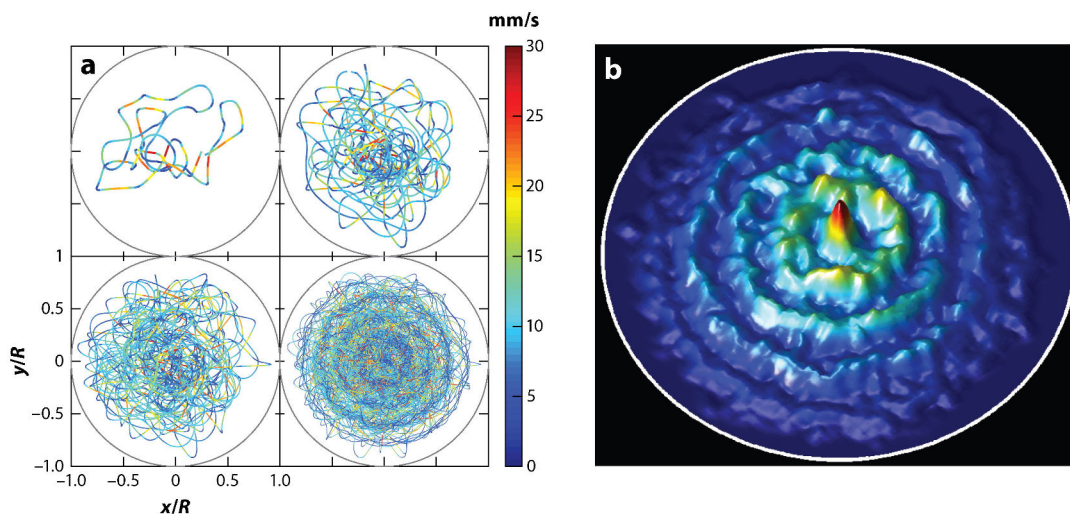


Figure 1.6: The figures show the motion of a single chaotic walker in a confined circular geometry. In (a) the path of the moving droplet is traced, where color indicates the velocity of the droplet. In (b) a histogram shows the droplet’s position within the circular corral over a span of time. A clear pattern emerges: the droplet appears to be contained within a statistical wave of wavelength  $\lambda_F$ . Adapted from J. W. M. Bush, *Annu. Rev. Fluid Mech.* **47**, 275 (2015).

to use the basketball/wall example as an analogy for the particle/barrier interaction because the “effective potential energy” of the brick wall is almost infinite, while that of the quantum potential barrier that allows tunneling, is not. For a high enough potential, the particle will also (almost) always bounce back. The point is that probabilistic tunneling cannot be seen at a classical scale in the way that is at the quantum scale, at least not until the discovery of the bouncing droplet system.

### Tunneling in the Bouncing Droplet System

A study performed by Eddi et al. examined tunneling in the bouncing droplet system [5]. In this setting, tunneling takes the form of the droplet tunneling through (or being reflected by) a submerged barrier. The droplet never actually travels through the barrier, since it bounces on the interface, but the analog to quantum tunneling remains because as the droplet approaches the barrier it is affected by the region of a different “potential”.

For a different depth of fluid  $H$ , a tray will have a different  $\gamma_W$ . If a tray has various regions of different depths, then these different regions will behave slightly differently. This means that when a walker travels from an area of one depth to an area of another depth, its behavior may change. This effect can be seen when a walker is pushed back from a submerged step, seemingly without any contact with the droplet. However, in certain cases, the walker will actually “tunnel” across the step; that is, it will continue to walk along the surface of the oil bath and pass into the new region of different depth, without reflection. Adjusting the width of the barrier as well

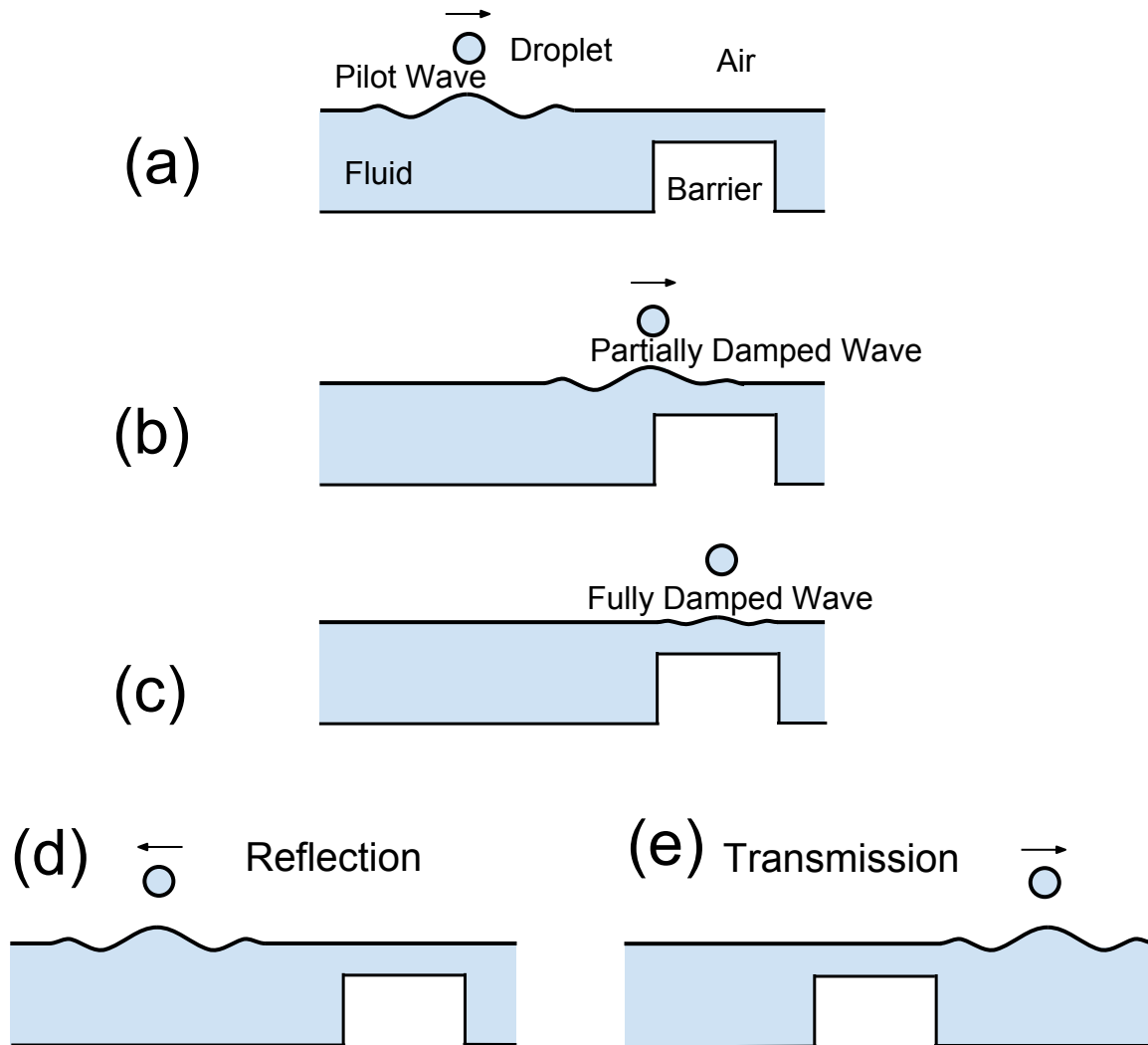


Figure 1.7: A diagram of the droplet-barrier interaction. In (a) the walker moves towards the barrier. As it gets closer (b), the guiding wave is damped. In (c) the guiding wave is fully damped such that the droplet is no longer a walker but a bouncer. Guided by the waves the droplet generated as a walker, the bouncer will either be reflected back from where it came (d), or carry on as shown in (e).

as its height will affect the behavior of the droplet. If we make the barrier of width  $e$  with height such that the depth of the oil above it is  $h$ , in a bath that otherwise has depth  $H$ , then we can think of it as a potential barrier. The unpredictability of the tunneling comes from the complex interaction between the drop and its guiding wave.

Now say we set  $\gamma$  such that walking occurs in the deeper section, but not in the more shallow section (i.e.  $\gamma_W(H) < \gamma < \gamma_W(h)$ ). Then, the droplet is simply a bouncer when in the shallow region, but a walker everywhere else. If the droplet starts out in the deeper region but crosses over to the shallow barrier, it slows down since it is no longer generating the self-propelling waves required for the walking

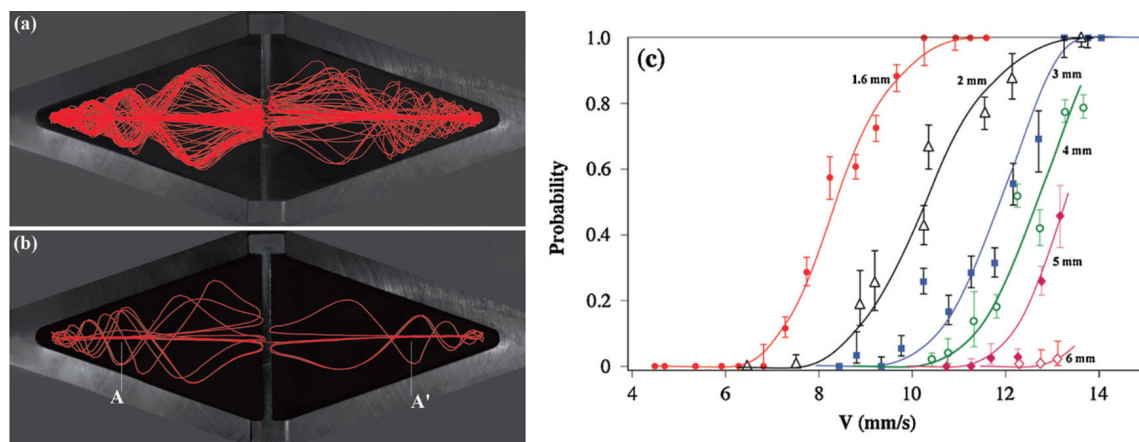


Figure 1.8: In (a) and (b) we see the path of a droplet traced out over many collisions with the barrier within rhombus shaped tray. The plot (c) shows the tunneling probability as a function of walker velocity for different barrier widths. Figures adapted from A. Eddi et al., *Phys. Rev. Lett.* **102**, 240401 (2009).

motion. Instead, the superposition of previous waves is what guides it either through or away from the barrier. However, if a droplet were to be created on the barrier, it would remain motionless. Therefore, we can understand the act of tunneling proceed as follows: the walker approaches a barrier, crosses the barrier as a bouncer, and eventually returns to the deeper region as a walker. The process is depicted in Fig. 1.7.

Eddi et al. built a tray with a submerged rhombus shape which forced the walker across the center of the tray as shown in Fig. 1.8 (a) - (b) [5]. A barrier was then placed along the diagonal of the rhombus, perpendicular to the direction of travel of the walker, so that the walker would run directly into the wall. They showed that as  $\gamma/\gamma_F$  approached 1, faster droplets had higher probabilities of tunneling (Fig. 1.8 (c)). They also discovered that by increasing the barrier width, the tunneling probability decreased.

The question that lingers, and that is the focus of this thesis, is the following: **How does tunneling probability change as a function of oil depth above the barrier  $h$ ?** We expect that at large  $h$  values the localized Faraday waves will be less damped, meaning that the walkers will tunnel more frequently. At small values of  $h$  where the localized Faraday waves are heavily damped, it is predicted that there will be very little tunneling. What is the critical height where we see both behaviors? An experiment, detailed in the following chapter, was designed to test this question.

# Chapter 2

## Experimental Design

In the bouncing droplet system we observe a unique interaction between a droplet and its wave that showcases various novel behaviors under different circumstances. In the experiments discussed herein, we will look at how features submerged beneath the surface of the oil affect the motion of the droplet.

A raised object on the floor of the tray (but still underneath the surface of the oil) can have an effect on height of the surface waves, and thus, on the motion of the walker [5]. Sometimes a droplet headed towards a raised object will be reflected backwards, as if from a collision with the object. For this reason, we refer to a submerged object as a barrier.

Oftentimes however, the droplet slows down, but continues on and crosses over the barrier without a collision. This is analogous to “transmission” in the quantum mechanical process of tunneling. For a barrier of a given height and width, there is a probability of tunneling unique to that barrier. Earlier studies have shown that increasing barrier width decreases probability of tunneling [5]. This study looks at how the height of the barrier affects the tunneling probability.

To test the effect of a barrier’s height on the probability of tunneling, I used a combination of procedures from the investigations of Bush et al. [1], Couder et al. [2], and specifically, Eddi et al. [5]. These were slightly modified to fit some of the unique features of my experiment. In this section, I aim to give some of the reasoning behind the design of the experimental apparatus and data collection techniques, both of which are not well described in the literature.

### 2.1 Setup

To guide the discussion of my experimental design, a schematic of the experimental setup is shown in Fig. 2.1 and a picture of the actual setup is shown in Fig. 2.3(a). In the experiment, a waveform generator creates a sinusoidal signal which is amplified and fed into a shaker. This signal drives the shaker, which vertically vibrates the tray containing the fluid. Both the frequency and the amplitude of the vertical oscillations can be controlled. An accelerometer records the vertical acceleration of the tray and is read using an oscilloscope. A CCD camera is used to record the droplet as it bounces

along the surface of the oil.

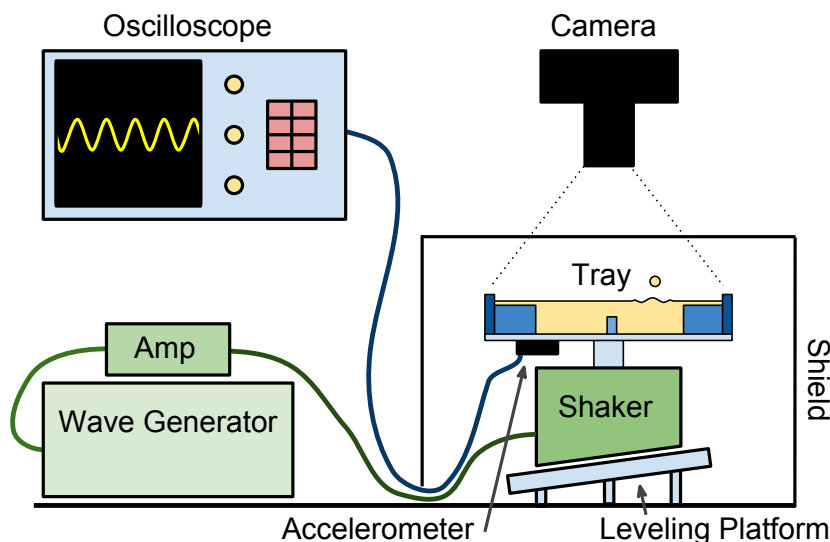


Figure 2.1: The experimental setup. The amplified signal from the wave generator drives the shaker, which shakes the oil-filled tray. The accelerometer generates a signal, which is read by the oscilloscope. The shield blocks disturbances to the experiment, while allowing the camera to document the trials.

## 2.2 Materials

The key components of this experiment are the shaker, the oil, and the tray. In this section I will describe the specifics of this holy trinity, as well as some of the additional components used in data collection.

### 2.2.1 Tray

The tray's design, which was based off of the tray in the tunneling experiment of Eddi et al. [5], naturally guides the droplet into a perpendicular collision with the barrier. The tray was fabricated from acrylic plastic parts that were cut on the Trotek Rayjet 300 laser cutter in Reed's machine shop. The manufactured components were then glued together with Scigrup Weld-On 3 assembly adhesive. A detailed schematic of the tray is shown in Fig. 2.2.

A thin layer of oil spills over the constraining rhombus shape. As long as the layer is thin enough, the droplet will remain in the rhombus container, but the waves will continue to propagate unimpeded. This gives the waves time to decay, meaning that the droplet's motion is not affected by reflections of previous waves from the sidewalls, and is instead guided only by the unreflected waves. The rhombus shape serves to steer the droplet into a perpendicular collision with the barrier. It does this by forcing the droplet to pin-ball into the acute corner of the rhombus so that it shoots out towards the barrier as shown in Fig. 2.3(c).

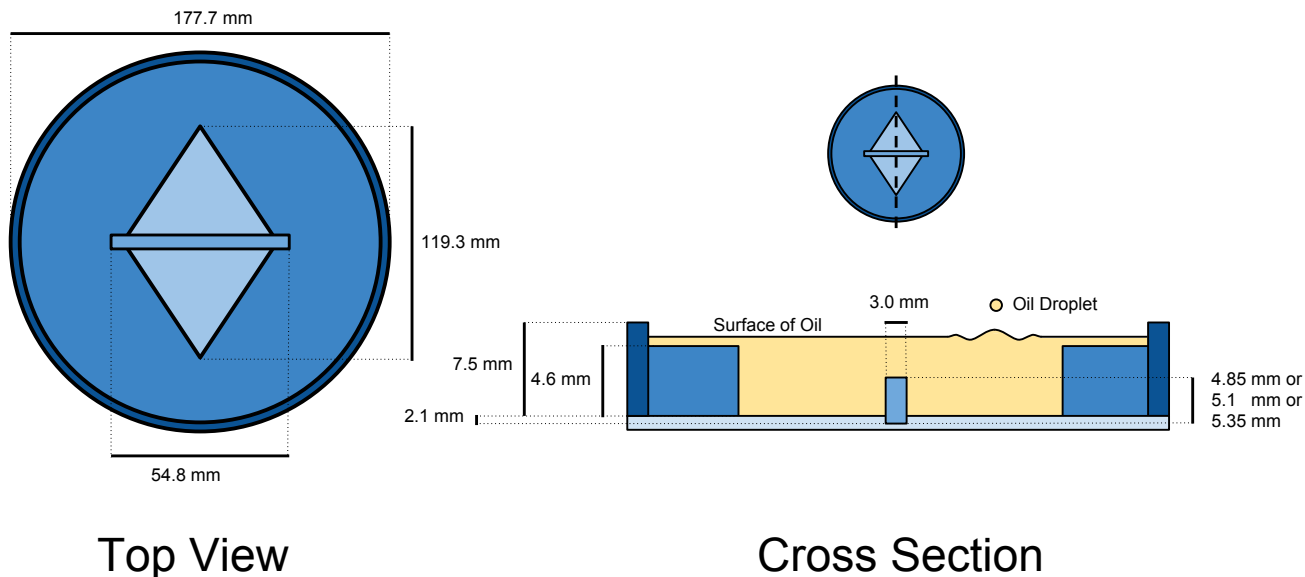


Figure 2.2: The specifications of the tray design. The top view (left) highlights the main elements in the tray. The cross section (right) illustrates the topography of the tray. The depth of the fluid layer is represented by the shading; darker shading is shallower.

We designed the experiment to test barriers of three different heights: 2.75 mm, 3.0 mm, and 3.25 mm, measured from the bottom of the rhombus. Thin acrylic barriers made by the laser cutter have a tendency to bend and warp over time. To avoid this problem, we made the barriers taller than the specified heights. Then we created a cut-out in the bottom of the rhombus so the barriers could be inserted and held in place by the tight fit. The barrier cut-outs were deep enough to exactly counter the added height of the barrier, so the barriers still had (when measured from the surface of the rhombus) heights of 2.75 mm, 3.0 mm, and 3.25 mm. This design also solved the problem of fixing the barriers in place, while allowing them to be easily removed. The particular heights of the barriers were chosen because they exhibited both transmission and reflection. Other barriers were also made but these were either too tall (3.5 and 4.0 mm) and blocked all of the droplets, or too short (1.0 and 2.0 mm) and did nothing to prevent the droplets from crossing over.

In order to improve contrast, the bottom of the tray was painted black, allowing the droplet to be more easily tracked by eye and when using a camera.

### 2.2.2 Silicone Oil

Silicone oil was the ideal choice of fluid for this experiment because it remains clean, it has a low vapor pressure (so it does not evaporate), and it can be purchased in a range of specific viscosities. The silicone oil used in this experiment had a viscosity of 20 centistokes (cSt) (its viscosity is a little closer to water than olive oil) and was purchased from Clearco Products Co. Inc., Bensalem PA (CAS No: 63148-62-9). 20

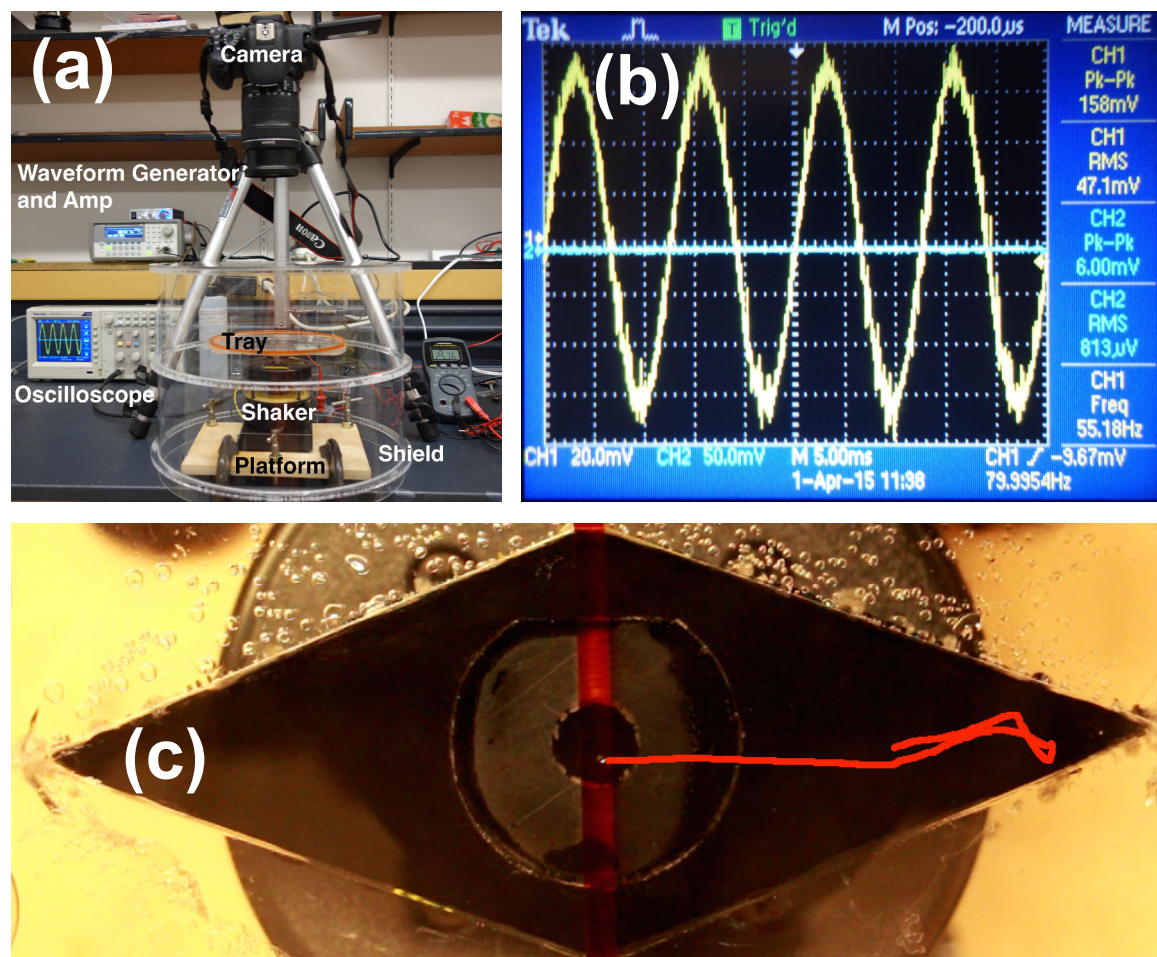


Figure 2.3: (a) The actual experimental setup. (b) The screen of the oscilloscope, showing the output from the accelerometer. The sine wave is proportional to the acceleration of the tray and has a frequency of 80.0 Hz and a peak to peak voltage of 158 mV. (c) The path of a droplet with a diameter of 0.87 mm, highlighted in red, shows the droplet's motion as it walks into a corner before shooting out directly towards the barrier (orange).

cSt silicone oil, like the one used by Bush et al. [1] was chosen because it exhibits walking behavior over a wider range of parameters [1] than more viscous oil, such as the 50 cSt viscosity oil used by Couder [2]. Depending on the height of the barrier and the desired height of oil above the barrier, the tray requires approximately 18.0 mL of fluid. This volume of oil left a different depth of oil above the barrier, depending on which barrier was in place. For the shortest barrier of 2.75 mm, the depth of the oil on top of the barrier was 1.5 mm. The intermediate barrier of height 3.0 mm had about 1.25 mm of fluid above it. The tallest barrier at 3.25 mm, only had 1.0 mm of fluid on top. The depths of the oil were calculated using the known oil volume and the dimensions of the tray.

It was of vital importance to keep the oil as clean as possible since surface contamination leads to droplet coalescence. This meant protecting the oil from particulate

matter that was already in the tray. Contamination was minimized by cleaning the tray before filling it and shielding it from the ambient dust using a plastic shield.

### 2.2.3 Shaker

To shake the tray, we used a mechanical wave driver made by Pasco Scientific, Roseville CA (model SF-9324). An acrylic component with a set screw was glued to the bottom of the tray. The tray was securely fastened to the thin rod that came on the shaker by tightening the screw.

This shaker is designed to drive a string or an elastic cord, not a 200 gram tray with oil inside. The combined weight of the tray and the oil resulted in a notable decrease in performance after just a couple of minutes of vibration. The initial behavior could be partially recovered after an hour long rest, but after weeks of use there was a noticeable difference. This difference was apparent in the acceleration measurements made by the accelerometer; towards the end of a trial, a signal with a higher amplitude had to be generated to produce the same accelerations measured at the beginning of the trial. For this reason, the shaker was replaced before collecting raw data and was allowed a resting period between trials. The damping of the vibrations also meant that the acceleration signals from the accelerometer had to be continuously monitored, since the constant signal from the wave generator could not be trusted to produce constant tray vibration.

### 2.2.4 Waveform Generator and Amplifier

The shaker was driven with an Agilent Arbitrary Waveform Generator (model 33210). This was controlled digitally and was found to be more stable than other available frequency generators available in the Physics department (e.g. Tektronix CFG280). The waveform generator was usually set to produce a sine wave at 80 Hz. The signal from the waveform generator was amplified using a Lepai LP2020A+ digital amplifier, which allowed precise control of the the amplitude of the tray. The signal, which was also monitored with a multimeter, was then fed into the shaker.

### 2.2.5 Accelerometer

As discussed in Chapter 1, knowing the tray's acceleration allows us to characterize the behavior of our system. To measure acceleration, we attached an ADXL 326 triple axis accelerometer (made by Adafruit, New York City NY) to the bottom of the tray using screws. This provided a much more secure mount than tape or glue while allowing for removal. The ADXL 326 has a range of  $\pm 16g$ , which was ideal for measuring the accelerations in our setup, which were usually below  $5g$ 's.

The signal from the z-axis of the accelerometer was measured directly on a Tektronix TDS 2012C oscilloscope. A sample output signal is shown in Fig. 2.3(b). For the vibrating tray, the output was approximately sinusoidal (as expected). The manufacturer's specifications for the accelerometer indicate a sensitivity of  $57 \pm 6$  mV/g.

### 2.2.6 Shield

A large, see-through cylinder (covered at one end) was manufactured using the laser cutter. When placed over the tray, it served the purpose of keeping the oil clean from particulate matter and preventing air currents from influencing the motion of the walker.

### 2.2.7 Leveling Platform

A wooden leveling platform supported the shaker. Three adjustment screws allowed for precise adjustment of the tilt of the apparatus. The alignment of the tray was tuned using a level placed inside the center of the tray (before the oil was added). This was done in order to ensure that the driving acceleration was aligned with gravity.

### 2.2.8 Camera

To document trials, we used a Canon EOS Rebel T5i DSLR camera supported on a tripod and aimed directly down at the tray. Attached to the camera was a Canon 18-135 mm lens. Set in its Tv configuration (Time Value – allows for shutter control) and in video mode, the 18 megapixel image could be optically zoomed and manually focused on the bouncing droplet. Other settings were left on automatic.

## 2.3 Procedure

Once the desired driving parameters were established (frequency and driving amplitude) so that walking behavior was observed, tunneling measurements at a few different barrier heights were made. These procedures are outlined in more detail below.

### 2.3.1 Finding the Walking Regime

Before investigating the rate of tunneling using different barriers, a rough estimate of the walking regime at a frequency of 80 Hz must be made. Using Fig. 1.2 as a guide for finding the walking parameters, an estimate of  $\gamma_F$  and  $\gamma_W$  was made. These values were expected to be slightly different from those found in the literature due to the slightly different height, tray, oil, and shaker configurations.

Droplet size is measured using a recorded video of the walking droplet in motion. By comparing the number of pixels making up the diameter of the droplet, which is unknown, to the number of pixels making up the known length of the diagonal of the rhombus, we can estimate the length associated with each pixel, and thus find the diameter of the droplet in millimeters. For accurate droplet diameter measurements, a mean value composed of 9 separate droplet diameter measurements per trial was computed. The droplets were found to have diameters on the order of 1.0 mm, as discussed in Section 1.1.

Driving acceleration values were measured by the accelerometer and displayed on the oscilloscope. To keep the acceleration constant throughout a measurement, the amplitude of the signal coming into the shaker was continuously adjusted in order to counteract the damping introduced as the shaker warmed up.

To ensure that every trial has the same oil depth, we measured the volume of oil (18.0 mL) before filling the tray using a 25 mL graduated cylinder with 0.5 mL graduation. Knowing the volume of the tray and of each barrier, we could calculate a value for the oil depth without interfering with the system. In this way, oil depth above the barrier (1.5 mm for the 2.75 mm barrier, 1.25 mm for the 3.0 mm barrier, 1.0 mm for the 3.25 mm barrier) could be made constant between trials.

### 2.3.2 The Experiment

This experiment utilized data collected from 3 independent trials. A trial consisted of measuring tunneling behavior for three different barrier heights using a single droplet. At each height (and at a constant frequency of 80 Hz and constant tray acceleration), a string of collisions were filmed with the camera. Between each measurement, the barriers had to be removed and replaced while the tray was still shaking in order to keep the droplet from coalescing. Since the size of the droplet changes its walking behavior, it was important to maintain a constant droplet diameter to allow for accurate comparisons between barrier heights. Not having a droplet of the same size is a major limitation to most of the research in the bouncing droplet system, such as in the other tunneling experiments [5], and the fact that we were able to keep ours constant is a great success. To maintain a constant memory,  $\gamma_F$  was measured for each system, and the value of  $\gamma$  was adjusted such that the  $\gamma/\gamma_F$  memory value stayed the same between barriers. From the collected data, a fraction of transmissions per total collisions was calculated, which provides the most simplistic tunneling analysis of this system.

The tray was designed such that most of the droplet's collisions with the barrier occur "head on" (i.e. perpendicular to the length of the barrier), but not all collisions unfold ideally. A more involved analysis using *Tracker* used the component of velocity of the droplet in the direction perpendicular to the barrier to determine the probability of tunneling given this value. Since not all collisions in the simplistic analysis occurred at the same velocity, the perpendicular velocity method provided a more refined analysis of the phenomenon.



# Chapter 3

## Data Analysis and Results

In this chapter, I will summarize the raw data and the corresponding results. The chapter ends with a discussion on the sources of error in the experiment.

### 3.1 Raw Data

The raw data consisted of a total of 7 videos. All of the variables collected for each trial are laid out in Table 3.1, and the raw data is presented in Table A in the **Appendix**. Barrier height, acceleration of the tray, Faraday threshold, and percentage of “transmissions” were recorded for each of the 7 videos. The 7 videos contained: one trial of a single droplet for all three barriers, a second trial of a single droplet for all three barriers, and a final trial of a single droplet for the 3.0 mm barrier.<sup>1</sup> By switching the barriers while the tray was still shaking we were able to use same droplet for each of the three barrier heights in a trial. There were between 12 to 24 separate collisions for each barrier. An example of a trial is presented in Fig. 3.1.

These movies were then processed with *Tracker* [22]. *Tracker* decomposes a video into multiple frames for the purpose of tracking an object in a video. The Autotracker function marks the position of the object in every frame and records the time in between each frame ( $\frac{1}{24}$  seconds). *Tracker* uses this information to estimate the velocity of the droplet at every frame. We also want to know the size of each droplet, so we measure the diameter of the droplet using a function in *Tracker*. The diameter is measured 3 times in each movie, yielding 9 total measurements per trial. These nine measurements were averaged to estimate the diameter of the droplet used in that trial. In trial 3, where only one barrier was used, 9 independent measurements were made, as detailed in Section 3.3.

From the volume of the oil  $V$ , which was measured with a graduated cylinder, and known dimensions of the tray, we can calculate the parameter  $h$ , which is defined as the height of the oil above the barrier. This was done by calculating the volume of the

---

<sup>1</sup>A similar methodology was attempted for Trial 3, but droplet coalescence prevented a complete trial from being recorded. Eventually it was decided to only examine the barrier with  $h = 1.25$  mm, since it exhibited the richest behavior.

Table 3.1: This table illustrates data collected for all trials. For each barrier (2.75 mm, 3.0 mm, or 3.25 mm), the forcing acceleration  $\gamma$ , the Faraday threshold acceleration  $\gamma_F$ , and the percentage of “transmissions” (%T) were recorded. The oil volume  $V$  was recorded at the beginning of each trial. From *Tracker*, measurements of the droplet diameter  $D_n$  in three randomly selected frames were made, along with the velocity of the droplet for every frame  $v(t)$ . Using  $V$ , the values of the depth of oil in the bath  $H$  and over the barrier  $h$  were calculated.

Trial	Barrier	Recorded	From <i>Tracker</i>	Calculated
1	2.75	$\gamma, \gamma_F, \%T, V$	3 x $D_1, v(t)$	$H, h$
	3.0	$\gamma, \gamma_F, \%T$	3 x $D_1, v(t)$	$H, h$
	3.25	$\gamma, \gamma_F, \%T$	3 x $D_1, v(t)$	$H, h$
2	2.75	$\gamma, \gamma_F, \%T, V$	3 x $D_2, v(t)$	$H, h$
	3.0	$\gamma, \gamma_F, \%T$	3 x $D_2, v(t)$	$H, h$
	3.25	$\gamma, \gamma_F, \%T$	3 x $D_2, v(t)$	$H, h$
3	3.0	$\gamma, \gamma_F, \%T, V$	9 x $D_3, v(t)$	$H, h$

“space” inside the tray, which required knowing the dimensions of the tray accurately. Values for the various parameters in this experiment are shown in Table 3.2. Error estimates are discussed in Section 3.3.

Table 3.2: Values of the various parameters in this experiment.

Parameter	Measured Value
Viscosity $\nu$ (cSt)	20.0 <sup>†</sup>
Frequency $f$ (Hz)	80.0
Density $\rho$ (g/mL)	0.95 <sup>†</sup>
Memory $\gamma/\gamma_F$	$0.98 \pm 0.03$
Drop Diameter $D$ (mm)	$0.99 \text{ to } 1.07 \pm 0.04$
Bath Depth $H$ (mm)	$4.26 \pm 0.04$
Oil Depth Above Barrier $h$ (mm)	$0.99 \text{ to } 1.52 \pm 0.04$

## 3.2 Analysis

### 3.2.1 Tunneling vs. Oil Depth

The primary purpose of this investigation was to determine how the depth of the fluid layer above the barrier affects tunneling. The results are shown in Fig. 3.2,

<sup>†</sup>Value provided by the manufacturer.

$$h_{2.75} = 1.51 \pm 0.04 \text{ mm}$$

$$T_{2.75} = 17/17 = 1.0$$

$$h_{3.0} = 1.26 \pm 0.04 \text{ mm}$$

$$T_{3.0} = 7/19 = 0.37$$

$$h_{3.25} = 1.02 \pm 0.03 \text{ mm}$$

$$T_{3.25} = 0/18 = 0.0$$

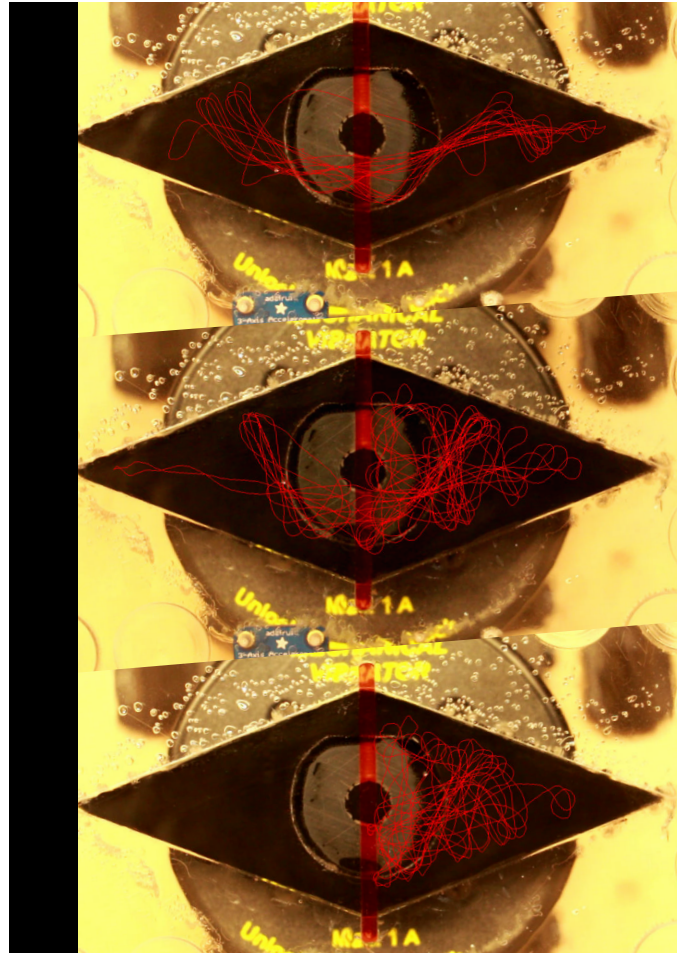


Figure 3.1: The the raw data from Trial 2. The red line in each image traces the path of the droplet for the duration of the trial. For each of the three barrier heights, the depth  $h$  of the oil above the barrier is shown, along with the fraction of droplets  $T$  that tunneled across the barrier.

indicating that droplets never crossed near  $h = 1.0$  mm, whereas they always crossed at  $h = 1.5$  mm. For the intermediate depth  $h = 1.25$  mm, both transmissions and reflections were observed at a rate that changes for every trial. If we consider the droplet diameter, we see that the plot suggests that the transmission coefficient increases as the diameter of the droplet increases.

### 3.2.2 Tunneling by Droplet Velocity

Not every droplet barrier collision was ideal. Many times, the droplets approached at an angle or at different velocities which means that it is a misleading to consider every collision as being the same. One way we can standardize collisions is by looking at the velocity perpendicular to the barrier at 5 mm away from the center of the barrier, as shown in Fig. 3.3.

We expect the perpendicular component of velocity to be important because it

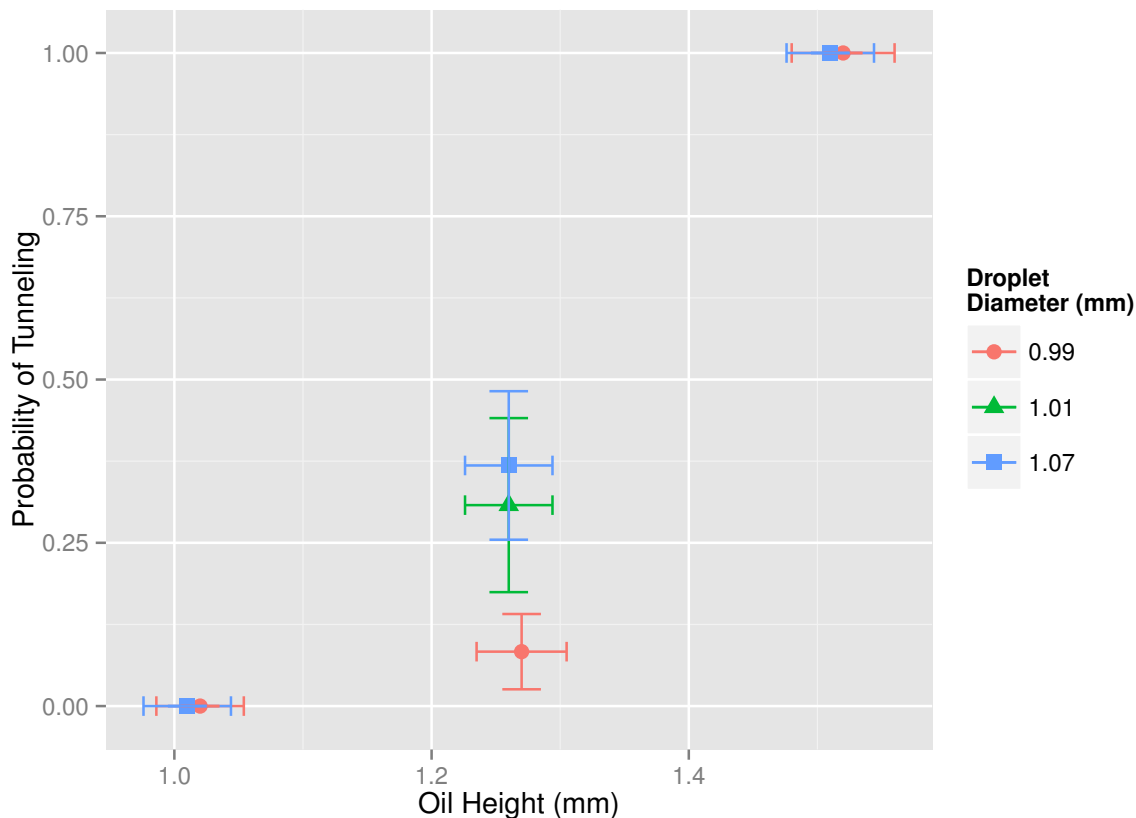


Figure 3.2: The proportion of collisions leading to transmission as a function of  $h$ . Each data series corresponds to a single trial for which the droplet diameter was kept constant. The vertical error bars indicate standard error, and the horizontal error bars indicate uncertainty calculated using error propagation.

proved critical in the study of barrier width carried out by Eddi et al. [5], and because intuitively, if the droplet moves faster, it has greater momentum and is more difficult to stop. Fig. 3.4 shows every collision for the intermediate barrier height, and the result of each interaction. In trials 2 and 3, the droplets with the fastest perpendicular velocities were usually the ones that passed through the barrier, as expected. This did not seem to be the case for trial 1, for unknown reasons.

Next, we try breaking up the collisions by velocity. The collisions from the 3.0 mm barrier were grouped into bins of width 2 mm/s and plotted by the fraction of all collisions that tunneled. The result, shown in Fig. 3.5, leaves a little to be desired. We see immediately the major limitation is the lack of trials, and perhaps, in consistency. Trial 3 is the only one that shows the expected trend for all bins: as velocity increases so does tunneling. Trial 2 starts off on the right track but a few reflections at high velocities skew the results. Finally, the results from trial 1 are inconsistent with the predicted behavior.

Our data seem to indicate that tunneling probability increases as a function of velocity and of droplet diameter. Droplet diameter is really just a way of expressing

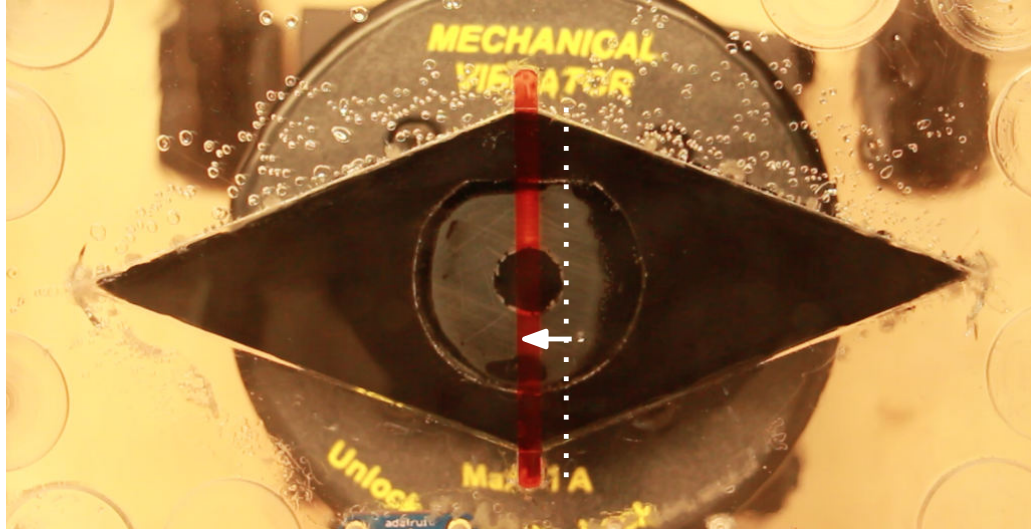


Figure 3.3: The image shows the point at which the measurement of the perpendicular component of velocity was made. This is 5 mm from the middle of the barrier.

the size of the droplet, but another way of doing that is by using the droplet's mass  $m$ . The momentum  $p$  of an object of mass  $m$  and velocity  $v$  is defined as:

$$p = mv.$$

We can estimate the mass of the droplet by multiplying the volume of the droplet by its density  $\rho$ . Assuming a spherical droplet of diameter  $D$ , the volume is given by:

$$V_d = \frac{4}{3}\pi \left(\frac{D}{2}\right)^3.$$

Thus, we can express the momentum of the droplet as

$$p_d = \rho V_d v \tag{3.1}$$

$$= \rho \frac{4}{3}\pi \left(\frac{D}{2}\right)^3 v \tag{3.2}$$

where the density  $\rho$  of silicone oil has been provided by the manufacturer. Looking at just the perpendicular component momentum and grouping the droplets into bins (as we did in Fig. 3.5 and then multiplying by the calculated mass  $m$  of the droplet) and we get the plot shown in Fig. 3.6. The plot shows incredibly similar slopes for portions of trials 2 and 3, suggesting the importance of momentum as a factor that increases tunneling probability. Even one of the momentum bins from the first trial falls on the curve, though the rest of the bins from that trial remain unexplained.

### 3.3 Sources of Error

With a system like the one studied here, which is sensitive to small variations in any parameter, it is crucial to keep track of the errors so that we can consider the

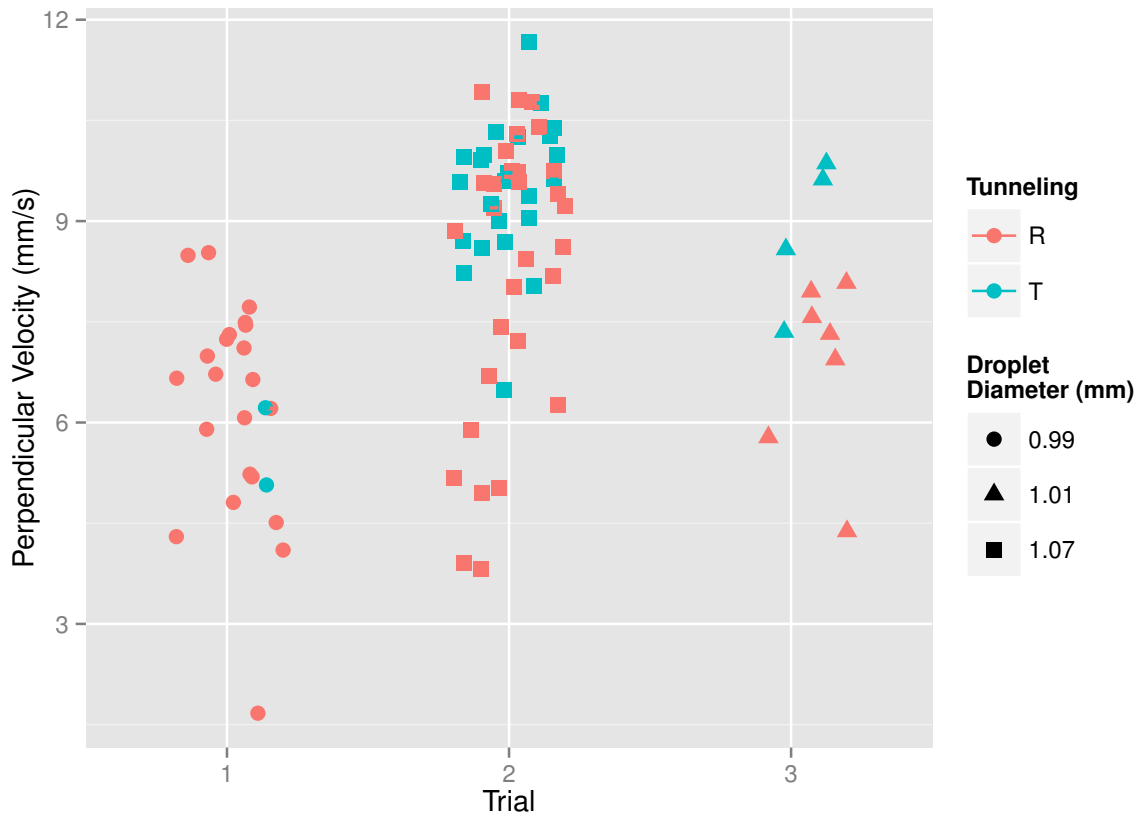


Figure 3.4: The result of each collision for the intermediate oil depth. The color represents the outcome of the collision (either transmission (T) or reflection (R)), and the shape represents the diameter of the droplet. The horizontal spread within each trial was added to aid in visualization.

limitations that these errors could have on our conclusions. Below, I discuss the nature of the experimental errors associated with my measurements.

### 3.3.1 Droplet Diameter

The droplet diameter measurements were made using the *Tracker* program. Knowing the length (in mm) of another object in the frame, in this case the length of the rhombus cutout inside the tray, we can measure the length of anything else in the frame (in mm). This works by finding the length in mm associated with each pixel in the frame and finding the width in pixels of the droplet. Using this ratio  $r_{\text{mtp}}$ , we can calculate the length of an object in mm:

$$\frac{\text{length of rhombus in mm}}{\text{length of rhombus pixels}} = r_{\text{mtp}} = \frac{\text{diameter of droplet in mm}}{\text{diameter of droplet in pixels}}$$

Since each pixel has a defined length, and because we cannot resolve anything within that pixel, our error is associated with that measurement is at least the width of half

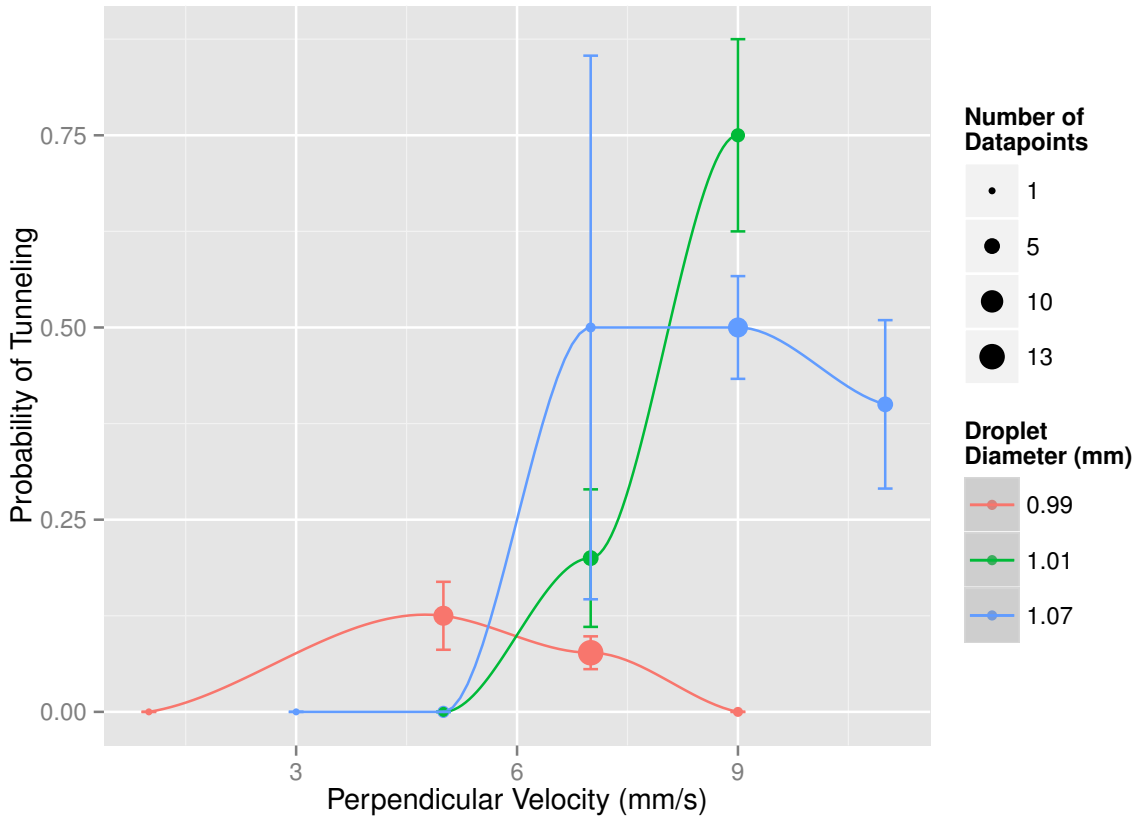


Figure 3.5: Collisions with similar perpendicular velocities were grouped into bins of width 2 mm/s per bin. The overall fraction of transmissions was computed for each bin, and plotted. Colors distinguish between droplet diameters, and sizes indicate the number of data points in each bin. Error bars indicate the associated standard error.

a pixel, usually around **0.04 mm**. There is also an error associated with the initial measurement of the rhombus in pixels, since it can be difficult to discern where exactly each point lies. This error was mitigated by making a new length measurement on *Tracker* every time the barrier was changed.

Additionally, the droplet does not remain a perfect sphere as it bounces. At the bottom of its bounce, the droplet will be squished and appear (from the top view) wider than usual, where at the moment of lift it will be less wide (from the top) than usual. Since the camera recording our data shoots at 24 frames per second, it is impossible to know at what point in the bounce the droplet is, so it is impossible to know when to measure the diameter of the droplet. For this reason, we measured the diameter of the droplet in 3 random frames at each of the 3 barrier heights, and with a total of 9 separate measurements per trial and averaged the results. Because the data for each barrier was filmed separately, this meant computing a new  $r_{\text{mtp}}$  value for each barrier. For the third trial in which only one barrier was used, the mm to pixel ratio  $r_{\text{mtp}}$  was re-calculated after 3 diameter measurements, in order to mimic the procedure of the first two trials. In other words, 3 separate groups of 3

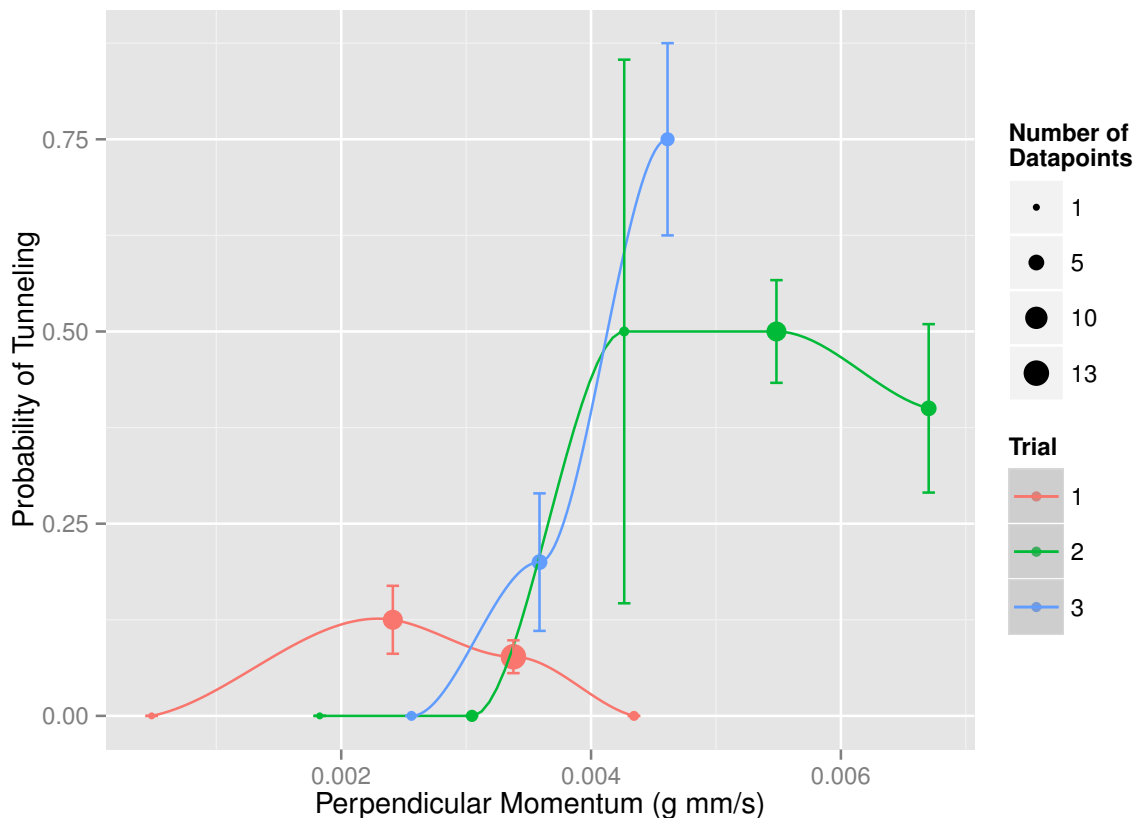


Figure 3.6: Collisions of similar perpendicular momentum were grouped into bins. The overall fraction of transmissions was computed for each bin, and plotted. Colors distinguish between trials, and sizes indicate the number of data points in each bin. Error bars indicate the associated standard error. The droplets were grouped by perpendicular velocities of width 2 mm/s per bin, and then these velocity values were multiplied by  $m$ .

measurements were made. Multiple measurements gave us an associated standard error, which combined with the error due to pixel limitations, gave us error bars.

Our measurement procedure helped reduce the error associated with the changing size during a bounce. It also reduced the error associated with finding the exact value of  $r_{\text{mtp}}$  since it was calculated 3 separate times each trial.

### 3.3.2 Droplet Velocity

The droplet velocity was measured using *Tracker*. The error in this measurement can be attributed to the Autotracker function, which automatically tracks the motion of the droplet using a built-in algorithm that searches a specific region of a frame for a known arrangement of pixels. Autotracking is mostly spot on, but if left alone for 1,000 frames, the marker begins to deviate from the actual location of the droplet. The marker was adjusted whenever a deviation was noticed. The error can be esti-

ated to no more than 10 pixels over 1000 frames, corresponding to  $\pm 0.01$  mm/s. We expect the error to be much lower than this in practice, since we are concerned only with a velocity measurement at a specific location 5 mm away from the barrier.

### 3.3.3 Height of Oil

The volume of oil was measured before each trial with a graduated cylinder with markings every half milliliter. With measurements on the order of 18.0 mL, there was an associated error of  $\pm 0.10$  mL. Then, oil was lost between barrier adjustments since pliers were inserted in the oil to pull each barrier out, and a little bit of oil remained on the barrier and on the pliers each time. The volume of fluid lost after each barrier replacement was estimated to be about 3 droplets of diameter 3.0 mm. This corresponds to a loss of **0.014 mL** of oil after every change in barrier. Finally, the volume of the oil was used to estimate the height of the oil above the barrier. The elements in the tray were manufactured for this experiment, and were then measured using digital calipers yielding an error of  $\pm 0.03$  mm.

For the height of the oil above the barrier, the above estimates provide us with an error on the order of about  $\pm 0.035$  mm. The amount of fluid lost after each barrier replacement corresponds to a depth  $H$  decrease of **0.002 mm** (for a barrier of the same size). This difference was offset by the added volume of the larger barrier, so that the bath depth  $H$  remained relatively constant across the entire trial.

It is impossible to account for factors such as the amount of oil left in the graduated cylinder, or the oil that may have seeped into microscopic fractures inside the tray. We assume these systematic errors to remain relatively constant over the duration of the experiment. This means that the pattern of our results should remain about the same, even if the exact numbers are slightly off.

### 3.3.4 Consistency of Memory

The shaker's acceleration decayed the longer it ran which lead to changes in droplet behavior. This could be seen by the acceleration measured by the accelerometer, which decreased even as the input signal remained constant. To counteract the changing acceleration, the amplitude of the driving signal was increased so that the system memory  $\gamma/\gamma_F$  remained constant (as measured by the accelerometer) throughout the duration of the experiment. After replacing each barrier, the Faraday threshold  $\gamma_F$  was re-measured. As the amount of oil and the barrier height changed, the Faraday threshold also changed, so keeping the same input signal was not an option. Rather, in all experiments the *memory* was kept constant, at  $\gamma/\gamma_F = 0.98 \pm 0.03$ . Because at different memories we see different droplet behaviors, a constant memory meant we keep the droplet behavior as consistent as possible over the course of a trial [20].

### 3.3.5 Imperfect Droplet Motion

The intent of the tray design was to create droplet trajectories such that their collisions were perpendicular to the length of the barrier. However, in practice, this was

not the case. Trajectories tended to deviate to one side and impacted the barriers at an angle. These trajectories tended to drift to the side of the tray with the accelerometer (shown in the top of Fig. 3.1), possibly because the accelerometer added weight to one side causing the tray to vibrate unevenly. Often, in situations in which the droplet was reflected, the trajectory would cycle through a triangular orbit before diverging off in another path. This meant for a couple of collisions in a row, the droplet-barrier collision was not ideal since it was not completely perpendicular.

The perpendicular velocity measurements were a work-around since they provide a more descriptive picture of each interaction. Even with this crutch though, the angled trajectories are a symptom of an imperfect setup. Though great care was taken to ensure that the tray was flat, it was impossible to adjust the mostly vertical direction of vibration to be perfectly vertical. When the oscillations are not exactly vertical, the oil inside the tray does not shake evenly and it is not at a constant depth throughout the tray, which leads to imperfect droplet motion. Rather than moving in a straight line until encountering a barrier of some sort, the droplet will slowly curl away from certain areas within the tray. Additionally, the tray in our setup was attached at a single point by a rod connected to the shaker. This could have led to bending of the acrylic at the edges, since the tray was so large. A mechanical shaker, as detailed in [23], would provide a much better base than the smaller shaker used in this experiment. It also would have the added benefit of shaking the entire tray at once, rather than just a single point. While the error due to this component cannot be measured quantitatively, it should be considered when drawing conclusions.

Despite these difficulties, we were able to show that barrier depth  $h$  did have an effect on the droplet's probability of tunneling, and that the mass and velocity of the droplet also played a role in determining this probability.

# Conclusion

The question we sought to answer was: How does tunneling probability of a walking droplet change with the depth of oil above the barrier? Our results showed that tunneling is highly sensitive in this system, and even changes in height on the order of fractions of a millimeter are enough to radically influence the proportion of tunneling droplets. Using a barrier of width  $e = 3.0$  mm, it was found that a depth of  $h = 1.5$  mm produced tunneling in every interaction, while at  $h = 1.0$  mm there was no tunneling. In the middle of this range was a sweet spot of  $h = 1.25$  mm where tunneling appeared probabilistic, but still somewhat dependent upon droplet diameter and droplet velocity. Our data suggests that for a given barrier, a droplet with a higher momentum is more likely to tunnel than a droplet with lower momentum. For a droplet of a constant diameter, tunneling occurs at higher values of  $h$ . The proportion of tunneling events decreases as the value of  $h$  decreases.

The main limitations in this investigation had to do with consistency of parameters between trials, and dearth of data points. The damping of the shaker made keeping consistent conditions in every trial difficult, and limited the number trials and interactions that were filmed. A better shaker would have significantly improved these things. For example, the shaker modeled in [23], shakes the whole tray at the same time and with same amplitude for hours. These shakers of course, cost more than the budget allowed for. Another difficulty was in measuring the height of the oil within a trial. When removing each barrier, a certain amount of oil was lost. While this value was estimated, it still was a source of uncertainty and it introduced contamination from the pliers into the oil (making coalescence likely).

## Future Work

An extension of this topic would benefit from using barriers of height 2.90 mm and 3.10 mm in addition to those used in this investigation, as this would have allowed for greater resolution in the tunneling probabilities as a function of  $h$ . Limitations in the shaker meant that testing more than three barriers using a single droplet became exceedingly difficult as the shaker's performance decayed, but an improved set up would make it possible.

Another avenue of study would be looking at how memory affected tunneling. For a constant barrier and a constant droplet, does adjusting memory affect the probability of tunneling? Because quantum-like behaviors emerge at higher memories we might expect these tunneling properties to exist only at these higher memories.

This experiment would be relatively easy to carry out since it uses a single barrier.

Finally, a few words of advice for those seeking to recreate the experiment: take your time in setting up the device, ensuring that the tray is level and that it vibrates vertically. Invest in good silicone oil, and do your best to limit any contamination of the oil. Finally, there is an accelerometer out there that does what you need, your task is simply to find it.

# Appendix

## Raw Data

The combined raw data is shown in Table A. The final two rows highlight the fact that the droplet diameter was measured 3 times for each of the 3 calculated  $r_{\text{ptm}}$  ratios.

Table A: The raw collected data.

Trial	$\gamma/\gamma_F$ (mV/mV)	%T	$D_{n,1}$ (mm)	$D_{n,2}$ (mm)	$D_{n,3}$ (mm)	$h$ (mm)
1	284 / 290	13/13	0.99	1.01	1.05	1.52
1	264 / 270	2/24	1.00	0.98	0.97	1.27
1	252 / 258	0/22	1.00	1.00	0.97	1.02
2	268 / 270	17/17	1.04	1.09	1.11	1.51
2	264 / 268	7/19	1.01	1.15	1.03	1.26
2	252 / 256	0/18	1.06	1.05	1.08	1.01
3	256 / 262	4/13	1.09	0.98	1.06	1.26
3	-	-	1.00	0.98	1.03	-
3	-	-	0.92	0.99	1.09	-



# References

- [1] J. W. M. Bush, “Pilot-wave hydrodynamics,” *Annu. Rev. Fluid Mech.*, vol. 47, p. 269, 2015.
- [2] Y. Couder, E. Fort, C.-H. Gautier, and A. Boudaoud, “From bouncing to floating: Noncoalescence of drops on a fluid bath,” *Phys. Rev. Lett.*, vol. 94, no. 17, p. 177801, 2005.
- [3] Y. Couder and E. Fort, “Single-particle diffraction and interference at a macroscopic scale,” *Phys. Rev. Lett.*, vol. 97, p. 154101, 2006.
- [4] A. U. Oza, D. M. Harris, R. R. Rosales, and J. W. M. Bush, “Pilot-wave dynamics in a rotating frame: On the emergence of orbital quantization,” *J. Fluid Mech.*, vol. 744, p. 404, 2014.
- [5] A. Eddi, E. Fort, F. Moisy, and Y. Couder, “Unpredictable tunneling of a classical wave-particle association,” *Phys. Rev. Lett.*, vol. 102, p. 240401, 2009.
- [6] Y. Couder, S. Protiere, E. Fort, and A. Boudaoud, “Dynamical phenomena: Walking and orbiting droplets,” *Nature*, vol. 437, no. 7056, p. 208, 2005.
- [7] L. de Broglie, “Ondes et quanta.,” *C. R.*, vol. 177, p. 507, 1923.
- [8] L. de Broglie, “Interpretation of quantum mechanics by the double solution theory,” *Ann. Fond. Louis Broglie*, vol. 12, p. 1, 1987.
- [9] D. Bohm, “A suggested interpretation of the quantum theory in terms of ‘hidden variables’ I,” *Phys. Rev.*, vol. 85, no. 2, p. 166, 1952.
- [10] D. Bohm, “A suggested interpretation of the quantum theory in terms of ‘hidden variables’ II,” *Phys. Rev.*, vol. 85, no. 2, p. 180, 1952.
- [11] J. Walker, “The amateur scientist,” *Sci. Amer.*, vol. 238, no. 6, p. 151, 1978.
- [12] M. Faraday, “On a peculiar class of acoustical figures; and on certain forms assumed by a group of particles upon vibrating elastic surfaces,” *Phil. Trans. R. Soc. Lond.*, vol. 121, p. 319, 1831.
- [13] K. Kumar, “Linear theory of Faraday instability in viscous liquids,” *Proc. R. Soc. A*, vol. 452, no. 1948, p. 1113, 1996.

- 
- [14] J. Moláček and J. W. M. Bush, “Drops walking on a vibrating bath: Towards a hydrodynamic pilot-wave theory,” *J. Fluid Mech.*, vol. 727, p. 612, 2013.
- [15] L. Rayleigh, “On the capillary phenomena of jets,” *Proc. R. Soc. Lond.*, vol. 29, p. 71, 1879.
- [16] S. Protiere, Y. Couder, E. Fort, and A. Boudaoud, “The self-organization of capillary wave sources,” *J. Phys.: Condens. Matter*, vol. 17, no. 45, p. S3529, 2005.
- [17] A. Eddi, D. Terwagne, E. Fort, and Y. Couder, “Wave propelled ratchets and drifting rafts,” *Europhys. Lett.*, vol. 82, no. 4, p. 44001, 2008.
- [18] S. Protiere, A. Boudard, and Y. Couder, “Particle-wave association on a fluid interface,” *J. Fluid Mech.*, vol. 554, p. 85, 2006.
- [19] A. Eddi, E. Sultan, J. Moukhtar, E. Fort, M. Rossi, and Y. Couder, “Information stored in Faraday waves: The origin of a path memory,” *J. Fluid Mech.*, vol. 674, p. 433, 2011.
- [20] D. M. Harris and J. Bush, “Droplets walking in a rotating frame: from quantized orbits to multimodal statistics,” *J. Fluid Mech.*, vol. 739, p. 444, 2013.
- [21] R. Brady and R. Anderson, “Why bouncing droplets are a pretty good model of quantum mechanics,” *arXiv*, 2014.
- [22] D. Brown, “Tracker video analysis and modeling tool.” <https://www.cabrillo.edu/~dbrown/tracker/>, November 2014.
- [23] D. M. Harris and J. Bush, “Generating uniaxial vibration with an electrodynamic shaker and external air bearing,” *J. Sound Vib.*, vol. 334, p. 255, 2015.